Copy
RM L53I14

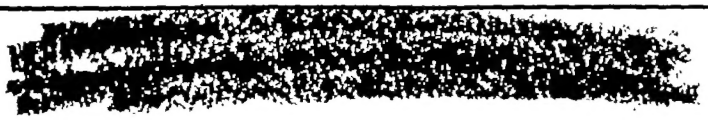

RESEARCH MEMORANDUM

AERODYNAMIC CHARACTERISTICS IN PITCH OF A SERIES OF CRUCIFORM-WING MISSILES WITH CANARD CONTROLS AT A MACH NUMBER OF 2.01

By M. Leroy Spearman

Langley Aeronautical Laboratory
Langley Field, Va.

NATIONAL ADVISORY COMMITTEE
FOR AERONAUTICS

WASHINGTON

October 30, 1953

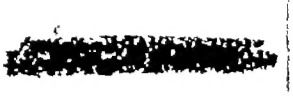

Unclassified

NASA Tech Pub Announcement #14

(NOTICE TO CHANGE)

3 March

NK

(SIGNATURE OF OFFICER MAKING CHANGE)

21 Feb. 61

DATE

NACA RM L53I14

NATIONAL ADVISORY COMMITTEE FOR AERONAUTICS

RESEARCH MEMORANDUM

AERODYNAMIC CHARACTERISTICS IN PITCH OF A SERIES OF CRUCIFORM-WING MISSILES WITH CANARD CONTROLS AT A MACH NUMBER OF 2.01

By M. Leroy Spearman

SUMMARY

An investigation has been conducted in the Langley 4- by 4-foot supersonic pressure tunnel at a Mach number of 2.01 to determine the static longitudinal stability and control characteristics of a series of missile configurations with canard controls at angles of attack up to about 28°. The missiles had cruciform wings and canard surfaces of delta plan form with 70° swept leading edges. Five bodies having fineness ratios of 19.1, 17.7, 16.7, 15.7, and 14.8 were investigated.

The results of the investigation indicated a large nonlinear variation of pitching moment with angle of attack for the body of largest fineness ratio that was progressively reduced by decreasing the fineness ratio until it was essentially eliminated for a body of fineness ratio 14.8. The increased linearity of the moment curve would make it possible to reduce the margin of stability so that, for a given canard size and deflection, a higher trim angle of attack might be obtained for the shortest missile than for the longest missile.

The pitching-moment results indicated that methods of prediction which assumed linear variations with angle of attack for the wing-alone and wing-plus-interference characteristics were adequate for angles of attack up to about 12°. At higher angles of attack it was evident that the characteristics of these components were nonlinear and that more refined methods would be required for adequate prediction.

INTRODUCTION

In connection with the development of missile configurations with canard controls an investigation has been conducted in the Langley 4- by 4-foot supersonic pressure tunnel to determine the aerodynamic

characteristics and interference effects for a series of such configurations at angles of attack up to about 28° and at high combined angles of attack and angles of sideslip. The models investigated had cruciform wings and canard surfaces of delta plan form with 70° swept leading edges and were equipped with all-movable canard surfaces for both pitch and yaw control and movable wing-tip ailerons for roll control. Various component parts of the models could be removed or changed in order to facilitate the investigation of general interference effects between different components and to permit the investigation of various modifications to the model.

Six-component force and moment measurements were made through an angle range from -2° to about 28° at various roll angles from 0° to 90°. A resolution of these results provides the aerodynamic characteristics for the missiles at angles of attack up to about 28° at zero sideslip or at combinations of angle of attack and angle of sideslip up to a maximum of about 20° for each.

This paper presents the results of tests made at a Mach number of 2.01 to determine the effect of body length on the longitudinal characteristics (zero roll angle) for five complete configurations as well as for the bodies alone, the bodies plus wings, and the bodies plus canard surfaces. The experimental results are compared with some simple theoretical estimates.

COEFFICIENTS AND SYMBOLS

The results of the tests are presented as standard NACA coefficients of forces and moments. The data are referred to the body-axis system (fig. 1) with the moment reference point for all configurations located 6.25 body diameters forward of the base of the body (-19.5 percent of the wing mean aerodynamic chord).

The coefficients and symbols are defined as follows:

C_N	normal-force coefficient (N/qS)
C_C	chord-force coefficient (C/qS)
C_m	pitching-moment coefficient $(M'/qS\bar{c})$
N	normal force
C	chord force

M'	pitching moment
q	free-stream dynamic pressure
S	total wing area resulting from extending the wing leading edge and trailing edge to the body center line
$\bar{c}$	wing mean aerodynamic chord
l_t	tail length measured from the moment reference point to the $\frac{2}{3}$-root-chord point of horizontal canard
x	distance from nose along body center line
Δx	longitudinal shift in moment reference point, positive rearward
M	Mach number
α	angle of attack, deg
α_{trim}	angle of attack at $C_m = 0$, deg
δ_H	horizontal-canard deflection, deg
C_{m_α}	rate of change of pitching-moment coefficient with angle of attack $\left(\partial C_m/\partial_\alpha\right)$
C_{m_δ}	rate of change of pitching-moment coefficient with horizontal canard deflection at $\alpha = 0^\circ$ $\left(\partial C_m/\partial \delta_H\right)$
$\alpha_{\delta_{trim}}$	rate of change of angle of attack with horizontal canard deflection at $C_m = 0$ $\left(\partial\alpha/\partial\delta_H\right)$

Subscript 45 refers to wing plane being rotated 45° with respect to the horizontal plane.

MODEL AND APPARATUS

Sketches of the models are shown in figure 2. The geometric characteristics of the models are presented in table I.

The body of the model was composed of a parabolic nose followed by a frustum of a cone which was faired into a cylinder. The body length was varied through the use of different lengths of the cylindrical portions inserted between the canard section and the wing section. Resulting

body fineness ratios were 19.1, 17.7, 16.7, 15.7, and 14.8. Coordinates for the body are given in table II. The canard surfaces and the wing had delta plan forms with 70° swept leading edges and hexagonal sections. The horizontal canard (pitch control) was motor-driven and deflections could be set by remote control.

Force measurements were made through the use of a 6-component internal strain-gage balance. The model was mounted in the tunnel on a remotely controllable rotary-type sting. The angle-of-attack range was from -2° to about 28°.

TESTS AND CORRECTIONS

Test Conditions

The conditions for the tests were:

Mach number	2.01
Reynolds number, based on $\bar{c}$	3.47×10^6
Stagnation pressure, atm	1.0
Stagnation temperature, °F	110

The stagnation dew point was maintained sufficiently low (-25°F or less) so that no condensation effects were encountered in the test section.

Corrections and Accuracy

The angle of attack was corrected for the deflection of the balance and sting under load. The Mach number variation in the test section was approximately ±0.01 and the flow-angle variation in the vertical and horizontal planes did not exceed about ±0.1°. No corrections were applied to the data to account for these flow variations. The base pressure was measured and the chord force was adjusted to a base pressure equal to the free-stream static pressure.

The estimated errors in the individual measured quantities are as follows:

C_N	±0.004
C_C	±0.002
C_m	±0.0004
α, deg	±0.1
δ_H, deg	±0.1

RESULTS AND DISCUSSION

The variation of C_N, C_C, and C_m with α is presented in figure 3 for the five complete model missile configurations. Data for wings rotated 45° are presented for models 1 and 4. Results for several values of δ_H are shown for all but model 5, for which data at only $\delta_H = 0°$ were obtained. The configurations for which results are presented are identified herein by the following designations:

Complete model (Body with wing and canard control)	BWC
Body with wing	BW
Body with canard control	BC
Body alone	B

A comparison of the variation of C_m with α for the different body lengths is shown in figure 4 for the BWC, BW, BC, and B configurations. It should be pointed out that these results are for a constant moment-reference-point location with respect to the base of the model; hence, the changes in the characteristics of the model result from changes in body length and canard location ahead of the moment reference point. The effects to be expected from varying the moment reference point are discussed subsequently.

The variation of C_N with α for the various component parts of the models is shown in figure 5. The estimated variation of C_N with α for the body alone (fig. 5(d)) was obtained by the method of reference 1. The estimated variation of C_N with α for the BW and BC configurations was obtained by the method suggested in reference 2 which entails combining the isolated wing or canard normal force (obtained in this case from ref. 3) and the normal force due to wing-body interference (ref. 2) with the body-alone results obtained by the method of reference 1.

The variation of C_C with α for the various configurations is presented in figure 6.

A breakdown of the pitching-moment characteristics of the various models is shown in figure 7. The estimated curve for the body alone was obtained by the method of reference 1. The center-of-pressure locations for the BW and BC configurations were obtained by the method of reference 4 and were used in conjunction with the estimated C_N values to determine the variation of C_m with α.

The constructed curves for the complete models obtained from the experimentally determined results for the component parts $[(BC - B) + BW]$ differ only slightly from the experimental results for the complete model. This result is an indication that all of the missiles are relatively free of canard wake and downwash effects. The minor effect on the pitching-moment variation with α resulting from rotating the wing 45° on models 1 and 4 (figs. 3(b) and 3(f)) is also an indication of little effect of the canard flow field on the wing. The variation of C_m with α for the complete models appears to depend largely upon the characteristics of the body alone for these configurations. However, a comparison between the experimentally determined and the estimated variation of C_m with α for the body-alone and body-wing configurations (fig. 7) indicates that even if the body-alone results could be predicted exactly, there would still be differences at angles of attack beyond about 12° for the body-wing configuration. The indications are that more consideration must be given to the estimated variations for the wing-alone and wing-plus-interfence results at higher angles of attack (which present theoretical methods considered to be linear) before more exact agreement between estimated and experimental results might be expected for the complete configurations.

The variation of the center-of-pressure location with angle of attack for each configuration as determined from the experimental results is shown in figure 8. The effects of these center-of-pressure variations will be apparent in the moment variations to be discussed later.

The variation of C_m at $\alpha = 0$ and α_{trim} with δ_H for models 1, 2, 3, and 4 is shown in figure 9. The variation of α_{trim} with δ_H for model 1 is that obtained from the stable portion of the pitching-moment curves only. At higher angles of attack second trim points are obtained which result in a negative slope of these curves. The moment-producing ability of the control is, of course, decreased with a decrease in moment arm. However, the fact that the pitching-moment variation with angle of attack becomes more linear as the body length is decreaed may make it possible to reduce the static margin for the shorter configurations so that the control effectiveness might be substantially increased. Some estimates have been made of the effect of shifting the moment reference (center-of-gravity) location by various amounts for models 1 and 5. The results (fig. 10) indicated that the variation of C_m with α for the short-body missile (model 5) would tend to become nonlinear when the static margin is reduced but to a slightly lesser extent than for the long-body missile (model 1). Conversely, when the stability of the long-body missile (model 1) was increased the moment variation became considerably more linear but was still less linear than for the short-body missile. The indications are, then, that although the effect of shortening

the body is not as great when equal low angle stability is considered, the moment variation for the shorter missile is still more linear than that for the longer missile.

An additional point to be considered in regard to the moment-reference location is that, from a geometrical or weight-distribution standpoint, it may be more practical to obtain the desired center-of-gravity location for the shorter missile than for the longer missile.

The variation with tail length of $\alpha_{\delta_{trim}}$, of C_{m_α} for the models with and without the wings, and of C_{m_δ} for the complete models at $\alpha = 0^\circ$ is presented in figure 11. The variations of C_{m_α} and C_{m_δ} with tail length are essentially linear. The negligible effect of the canard wake on the wing is shown by the fact that the variation of C_{m_α} with tail length is the same either with or without the wing.

For linear variations of C_{m_α} and for constant values of C_{m_δ} with α, the control-effectiveness parameter α_δ may be determined simply as $\alpha_\delta = \frac{C_{m_\delta}}{C_{m_\alpha}}$. However, the values of $\alpha_{\delta_{trim}}$ obtained experimentally (fig. 11) are equivalent to about 0.9 $\frac{C_{m_\delta}}{C_{m_\alpha}}$ because C_{m_δ} decreases with α. The relation $\alpha_\delta = 0.9\left(\frac{C_{m_\delta}}{C_{m_\alpha}}\right)$ might be used, then, to estimate the control effectiveness for different moment reference locations. For this purpose the variation of C_{m_α} with moment reference location as obtained from figure 10 has been included on figure 11 for models 1 and 5. These variations in C_{m_α} are much greater than those shown for the different body lengths since relocation of the moment reference point results in a change in the moment arm to the wing normal force which is the predominant normal-force component. The variation of C_{m_δ} with tail length at $\alpha = 0$ will be the same regardless of whether the moment reference location is shifted or the body length is changed. It was estimated that a moment reference shift of $-0.1\bar{c}$ would be required for model 1 in order to prevent the occurrence of second trim points and that a shift in the moment reference point of $0.2\bar{c}$ could be tolerated for model 5 without the occurrence of second trim points. Using the values of C_{m_δ} and C_{m_α} for these changes in the moment reference location, the resulting $\alpha_{\delta_{trim}}$ was found to be 0.74 for model 5 and 0.58 for model 1. The indication is, then, that because of the more linear variation of C_m with

α for the shorter missile a higher usable $\alpha_{\delta_{trim}}$ can be obtained than can be had for the longer missile.

CONCLUDING REMARKS

The results of tests made at a Mach number of 2.01 of the aerodynamic characteristics in pitch for a series of missile configurations with canard controls and body fineness ratios varying from 19.1 to 14.8 indicated that the canard wake effects were small and that the static longitudinal stability characteristics were influenced considerably by the characteristics of the body alone.

A large nonlinear variation of pitching moment with angle of attack for the longest body configuration tested (fineness ratio 19.1) was progressively reduced by shortening the body length until it was essentially eliminated for a body of fineness ratio 14.8. This reduction in length resulted in a decrease in the pitching effectiveness of the canard control but the increased stability and the linearity of the moment variation with angle of attack was such that a reduction in static margin could be permitted so that the usable trim angle-of-attack variation with control deflection would be higher for the shortest missile than for the longest missile.

The pitching-moment results indicated that methods of prediction which assumed linear variations with angle of attack for the wing-alone and wing-plus-interference characteristics were adequate for angles of attack up to about 12°. At higher angles of attack it was evident that the characteristics of these components were nonlinear and that more refined methods would be required for adequate prediction.

Langley Aeronautical Laboratory,
National Advisory Committee for Aeronautics,
Langley Field, Va., August 25, 1953.

REFERENCES

1. Allen, H. Julian: Estimation of the Forces and Moments Acting on Inclined Bodies of Revolution of High Fineness Ratio. NACA RM A9I26, 1949.

2. Nielsen, Jack N., and Kaattari, George E.: Method for Estimating Lift Interference of Wing-Body Combinations at Supersonic Speeds. NACA RM A51J04, 1951.

3. Ribner, Herbert S., and Malvestuto, Frank S., Jr.: Stability Derivatives of Triangular Wings at Supersonic Speeds. NACA Rep. 908, 1948. (Supersedes NACA TN 1572.).

4. Kaattari, George E., Nielsen, Jack N., and Pitts, William C.: Method for Estimating Pitching-Moment Interference of Wing-Body Combinations at Supersonic Speed. NACA RM A52B06, 1952.

TABLE I

GEOMETRIC CHARACTERISTICS OF MODEL

Wings:	
Span, in.	11.853
Chord at body center line, in.	17.069
Chord at body intersection, in.	13.407
Area (leading and trailing edges extended to body center line) sq in.	104.8
Area (exposed) sq in.	64.16
Aspect ratio	1.404
Sweep angle of leading edge, deg	70
Thickness ratio at body center line	.0147
Leading-edge angle normal to leading edge, deg	15.6
Trailing-edge angle normal to trailing edge, deg	7.4
Mean aerodynamic chord, in.	11.48
Canard surfaces:	
Area (exposed) sq. in.	6.406
Aspect ratio	1.73
Sweep angle of leading edge, deg	70
Mean aerodynamic chord, in.	2.576
Body:	
Maximum diameter, in.	2.666
Base area, sq. in.	5.583
Length (model 1), in.	50.833
Length (model 2), in.	47.333
Length (model 3), in.	44.667
Length (model 4), in.	42.000
Length (model 5), in.	39.565
Fineness ratio (model 1)	19.1
Fineness ratio (model 2)	17.7
Fineness ratio (model 3)	16.7
Fineness ratio (model 4)	15.7
Fineness ratio (model 5)	14.8

TABLE II

BODY COORDINATES IN INCHES

Body station		Radius	
0	(Nose)	0	
.297		.076	
.627		.156	
.956		.233	
1.285		.307	
1.615		.378	
1.945		.445	
2.275		.509	
2.605		.573	
2.936		.627	
3.267		.682	
3.598		.732	
3.929		.780	
4.260		.824	
4.592		.865	
4.923		.903	
5.255		.940	
5.587		.968	
5.920		.996	
6.252		1.020	
6.583		1.042	Conical section
11.542		1.333	Conical section
50.833		1.333	Cylindrical

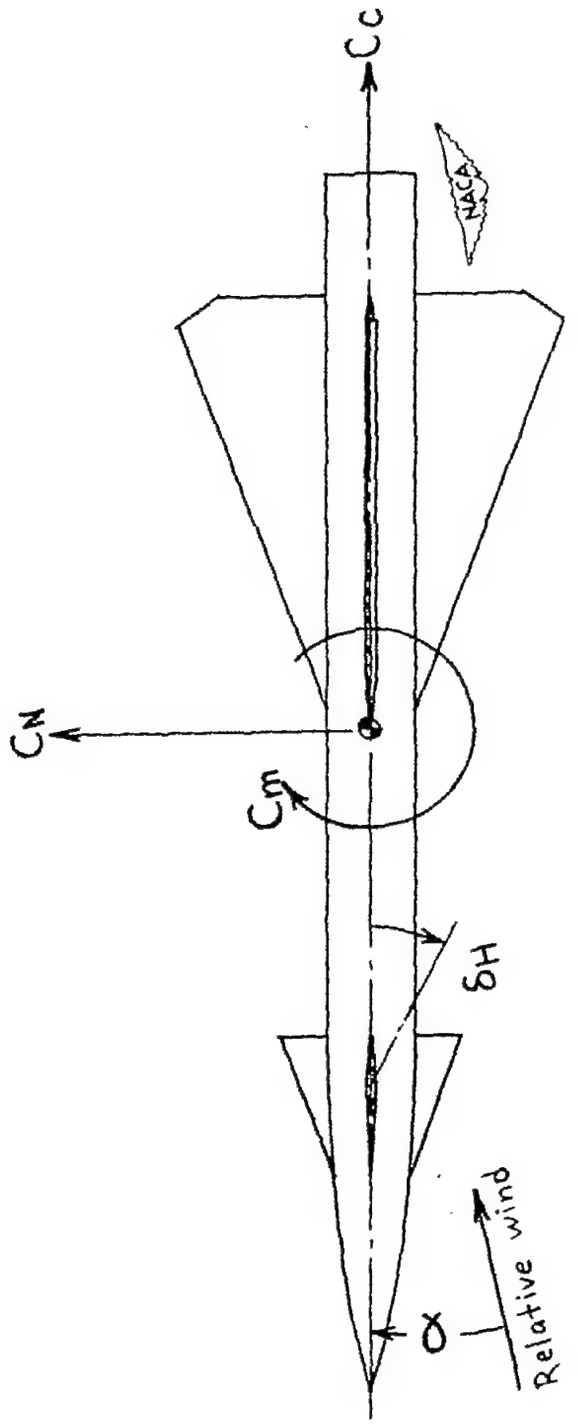

Figure 1.- System of body axes. Arrows indicate positive values and directions.

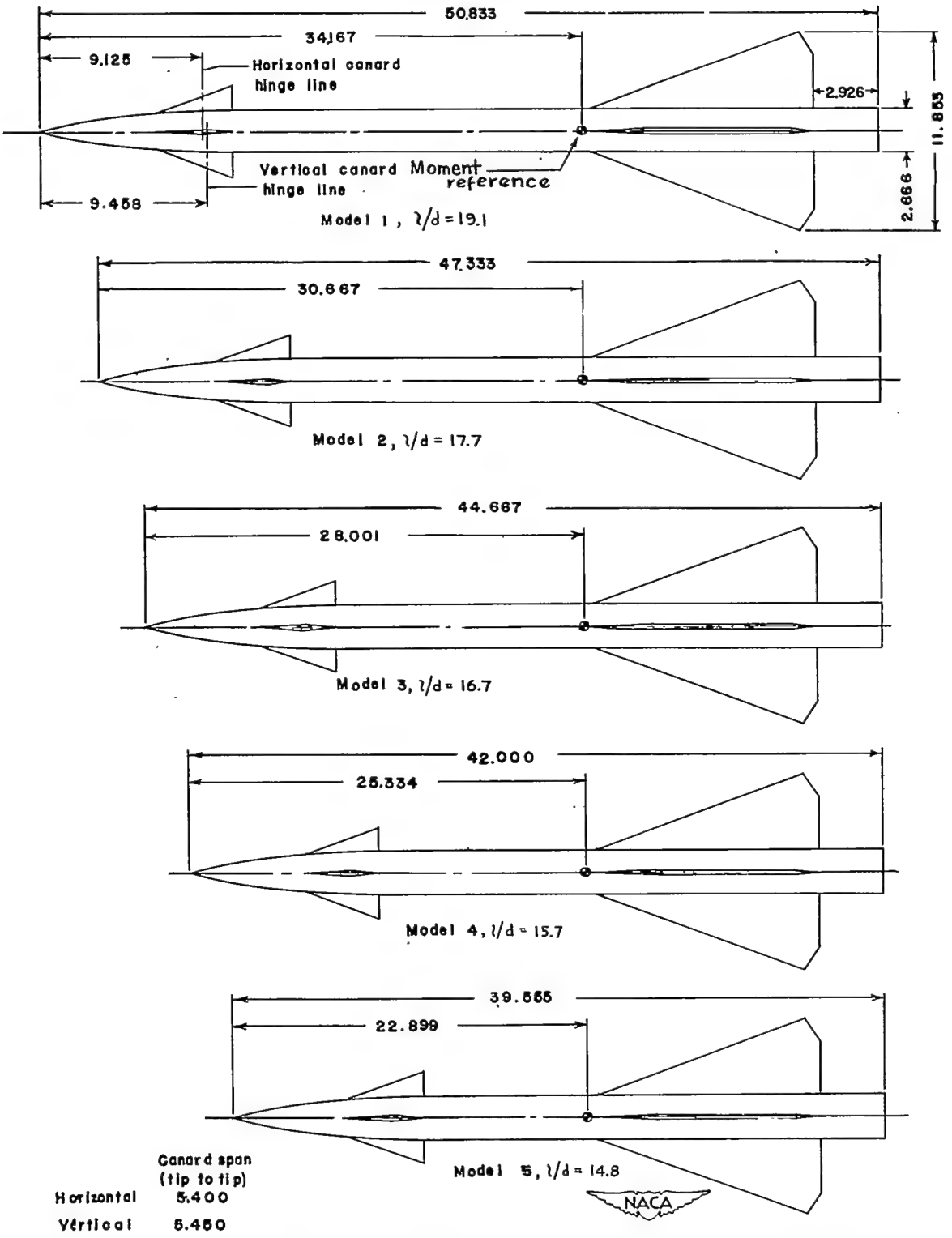

Figure 2.- Details of models. (All dimensions in inches.)

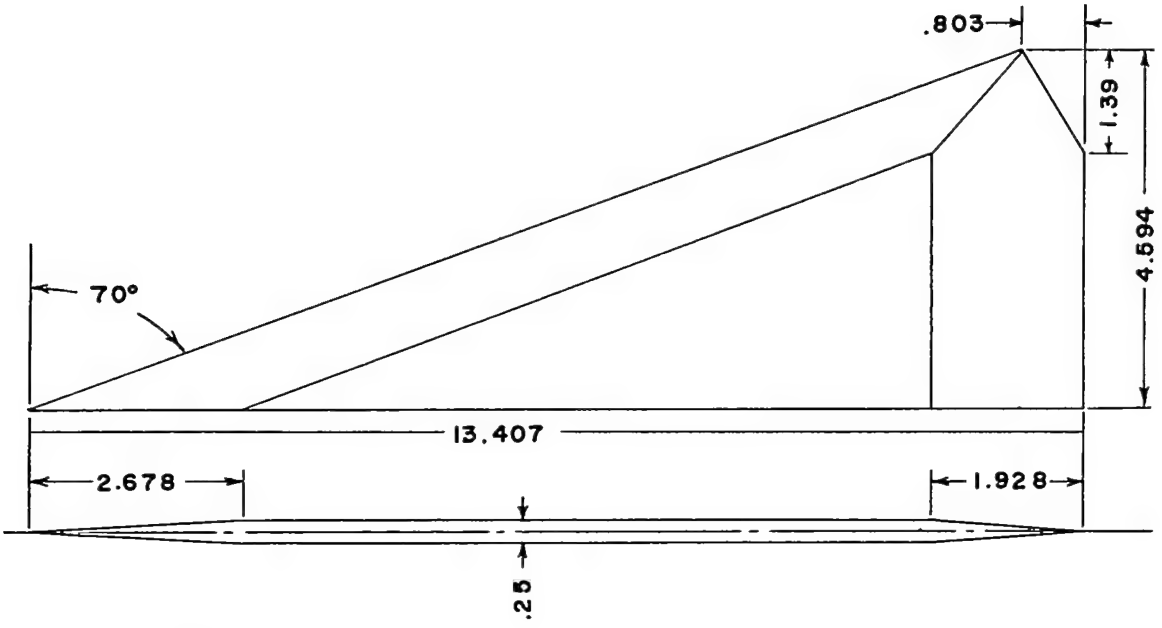

Wing panel

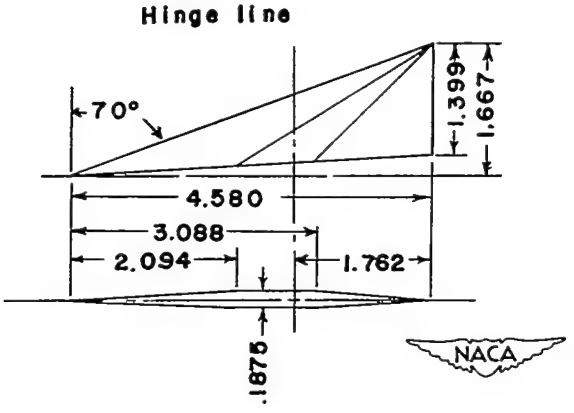

Canard control panel

Figure 2.- Concluded.

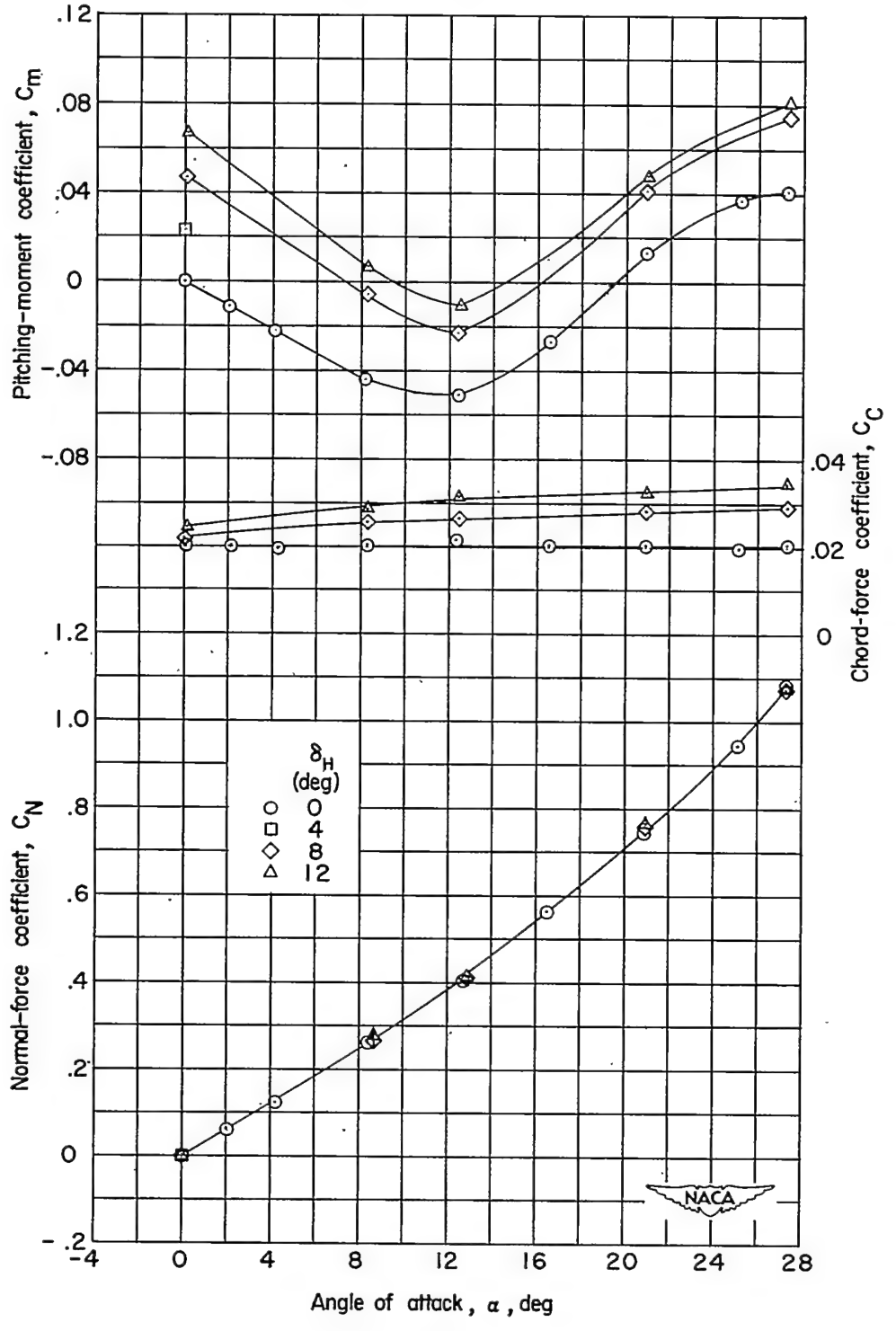

(a) Model 1; l/d = 19.1.

Figure 3.- Aerodynamic characteristics in pitch for various complete model configurations.

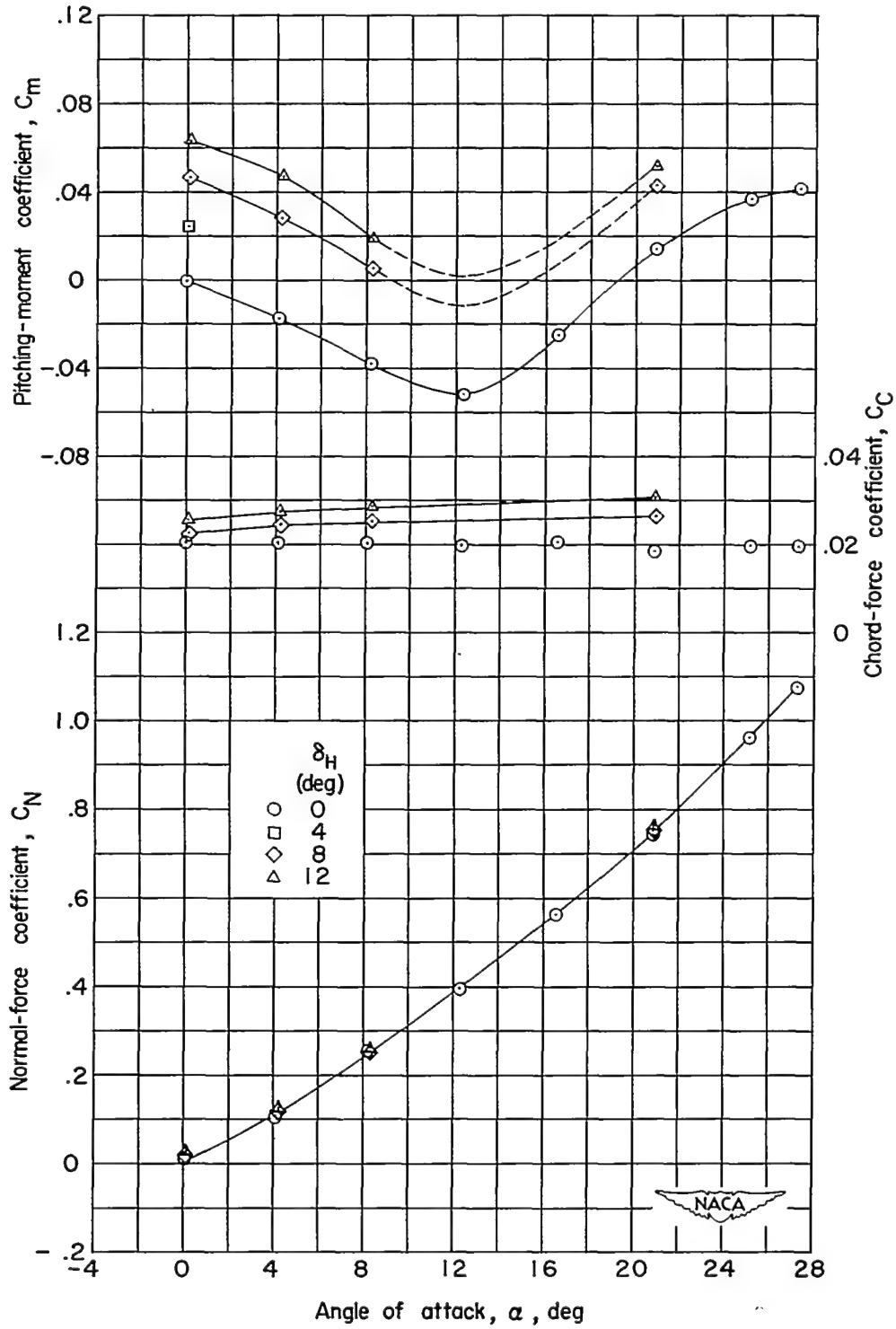

(b) Model 1 with wings rotated 45°.

Figure 3.- Continued.

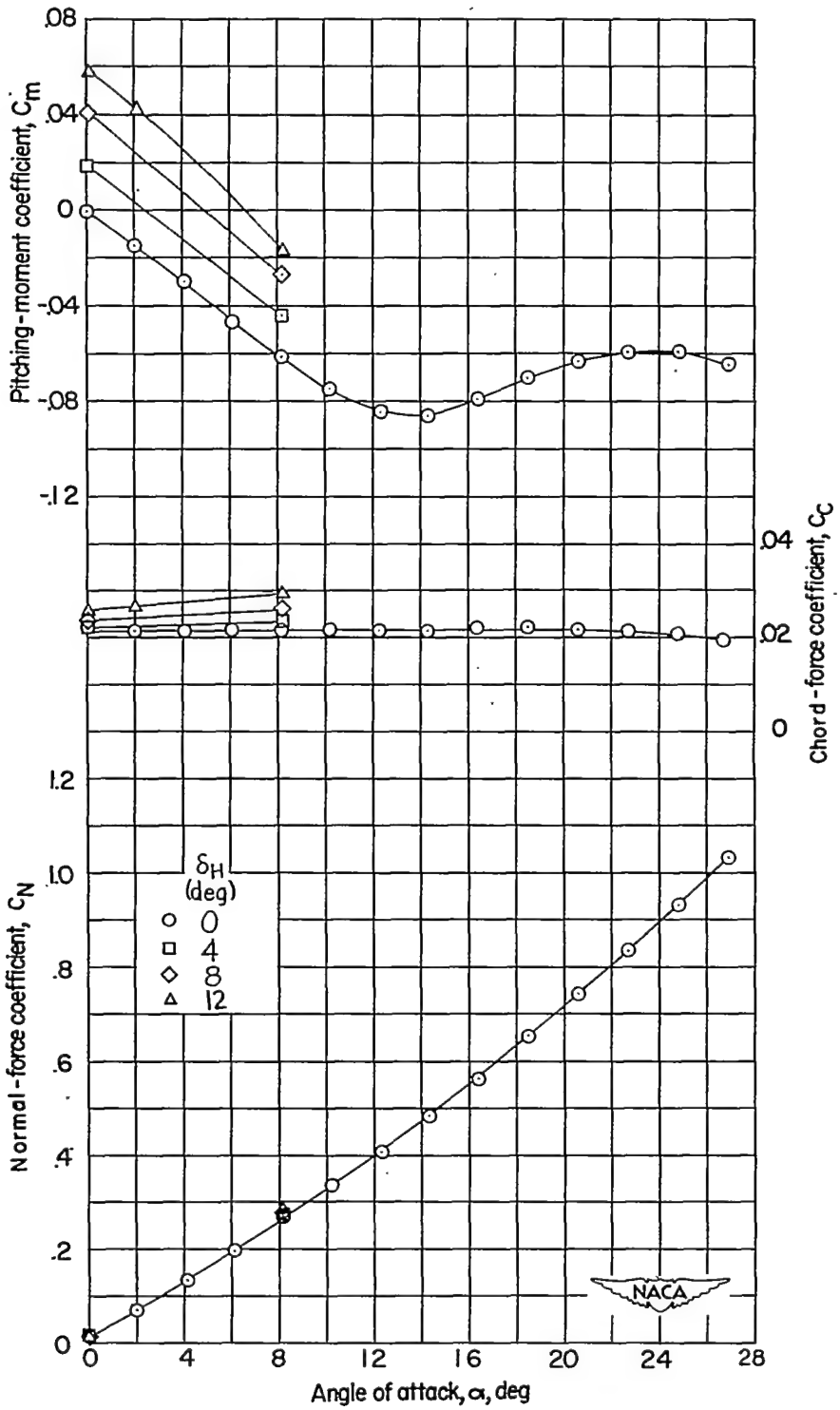

(c) Model 2; $l/d = 17.7$.

Figure 3.- Continued.

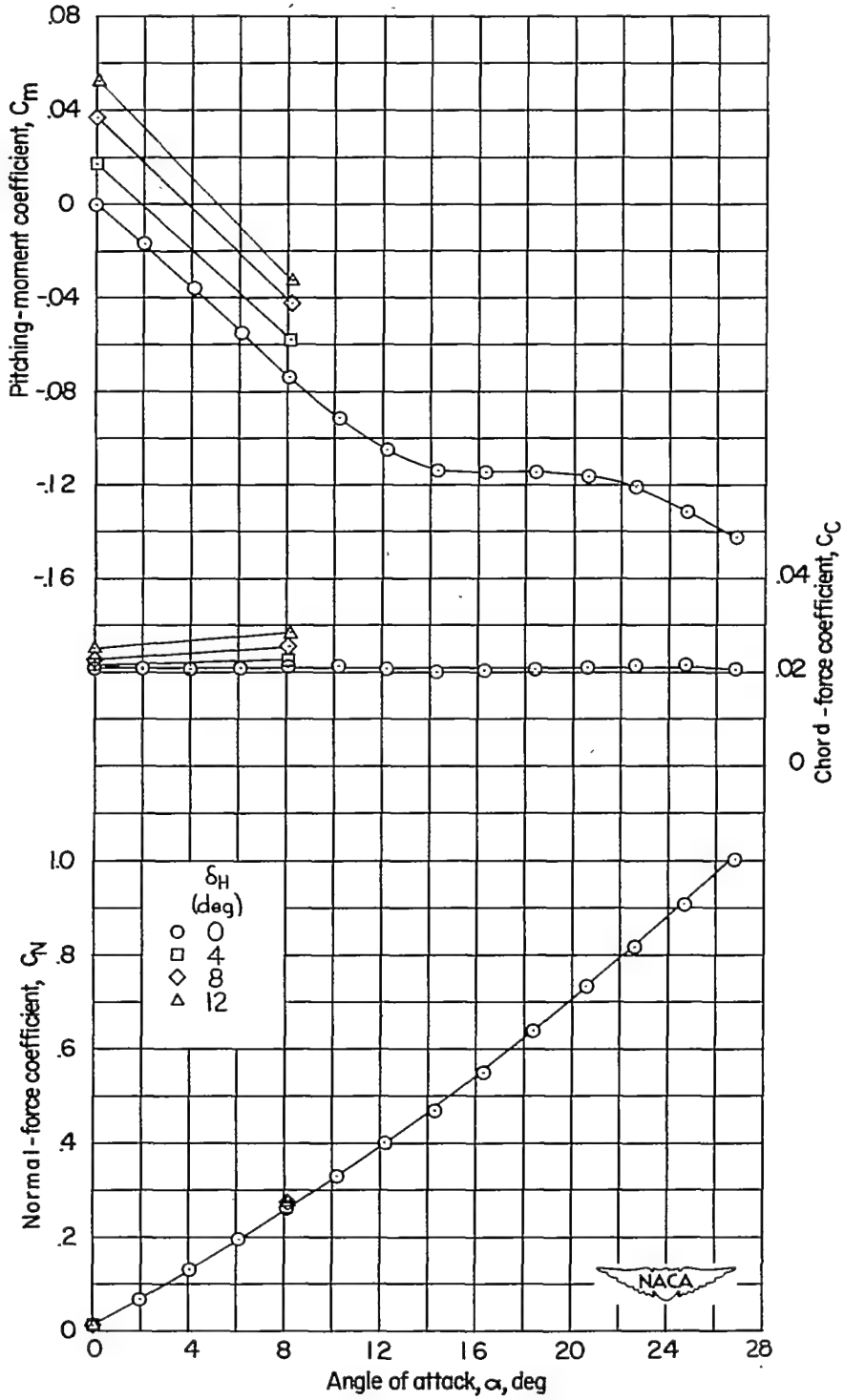

(d) Model 3; $l/d = 16.7$.

Figure 3.- Continued.

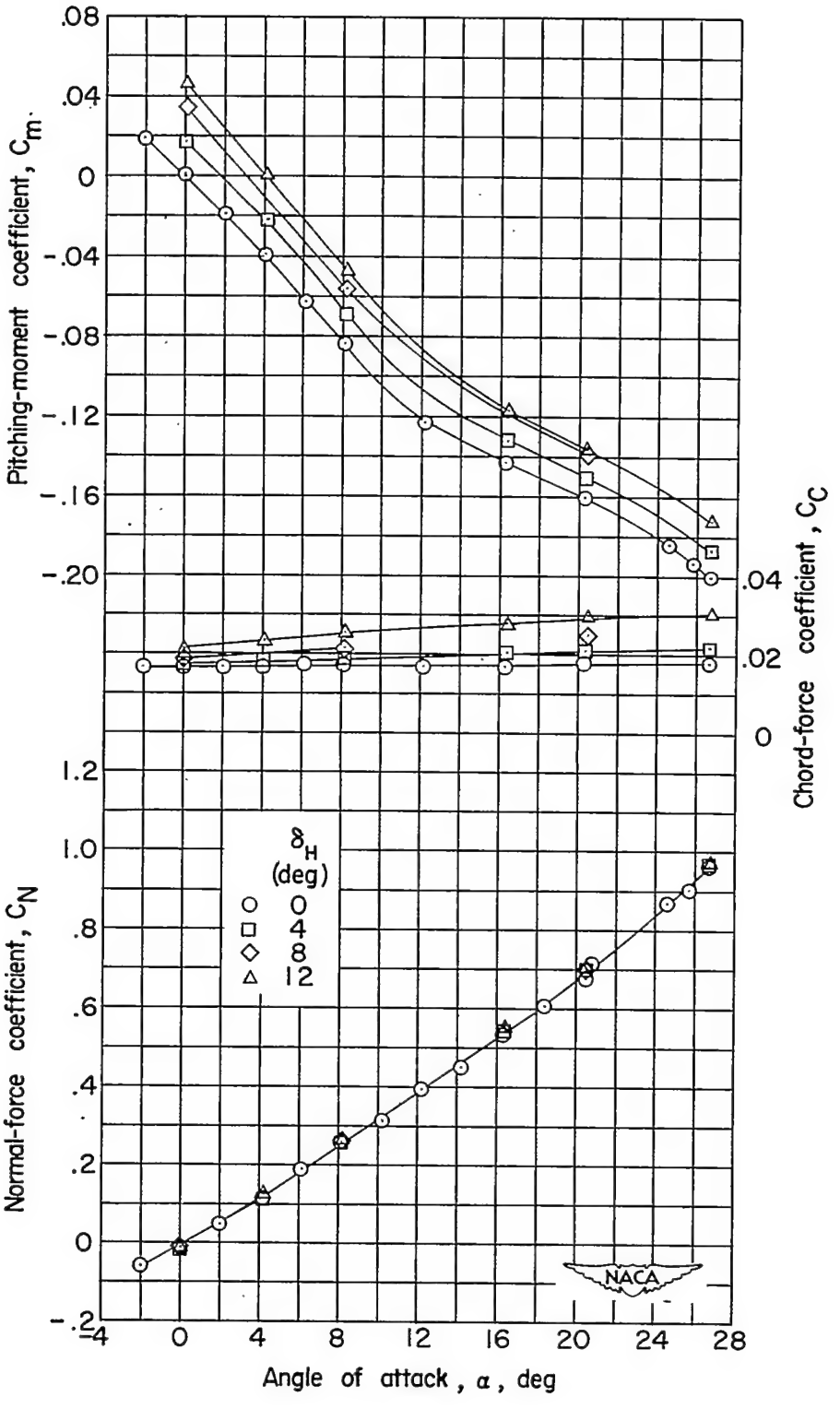

(e) Model 4; $l/d = 15.7$.

Figure 3.- Continued.

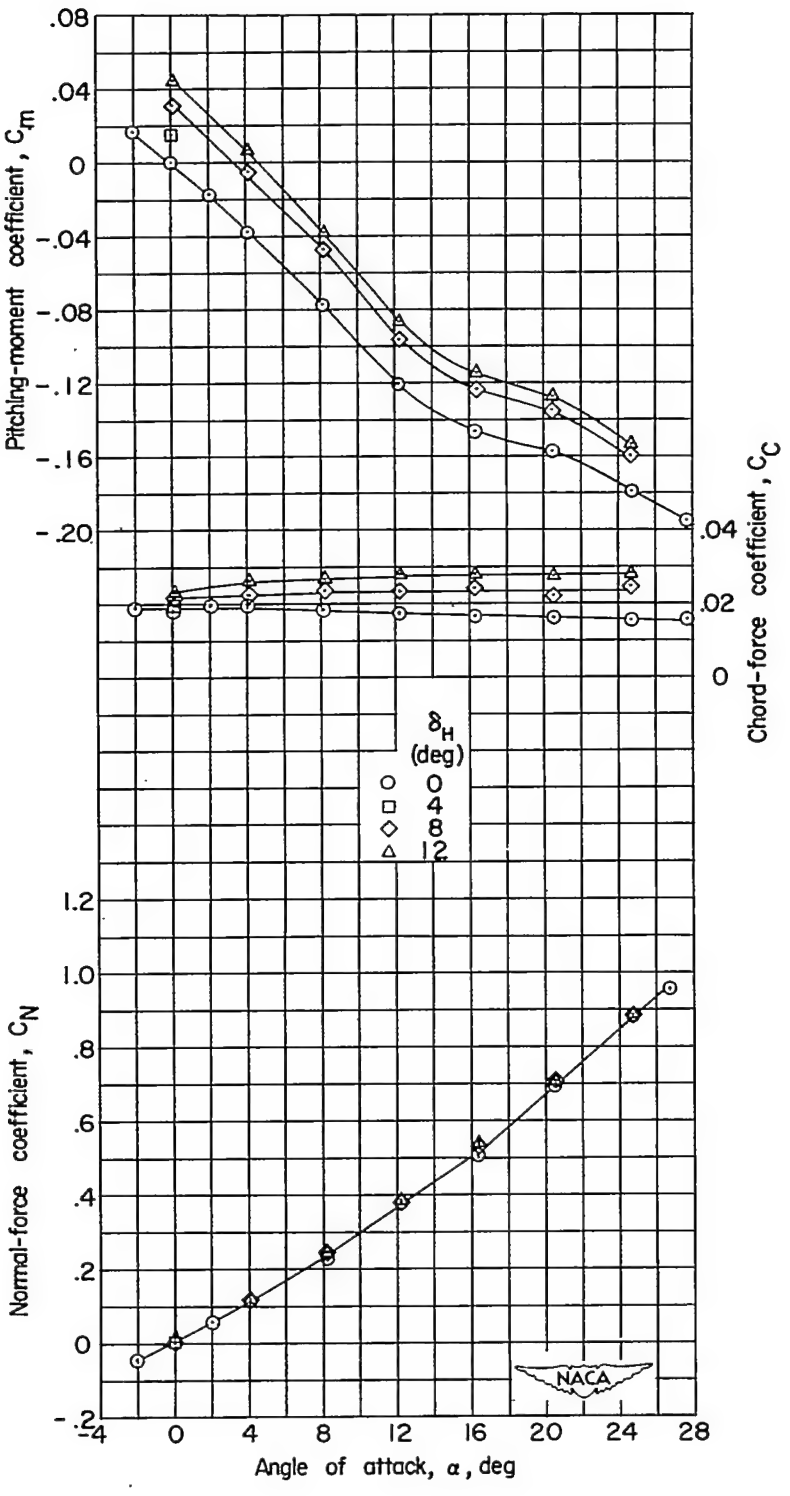

(f) Model 4; wings rotated 45°.

Figure 3.- Continued.

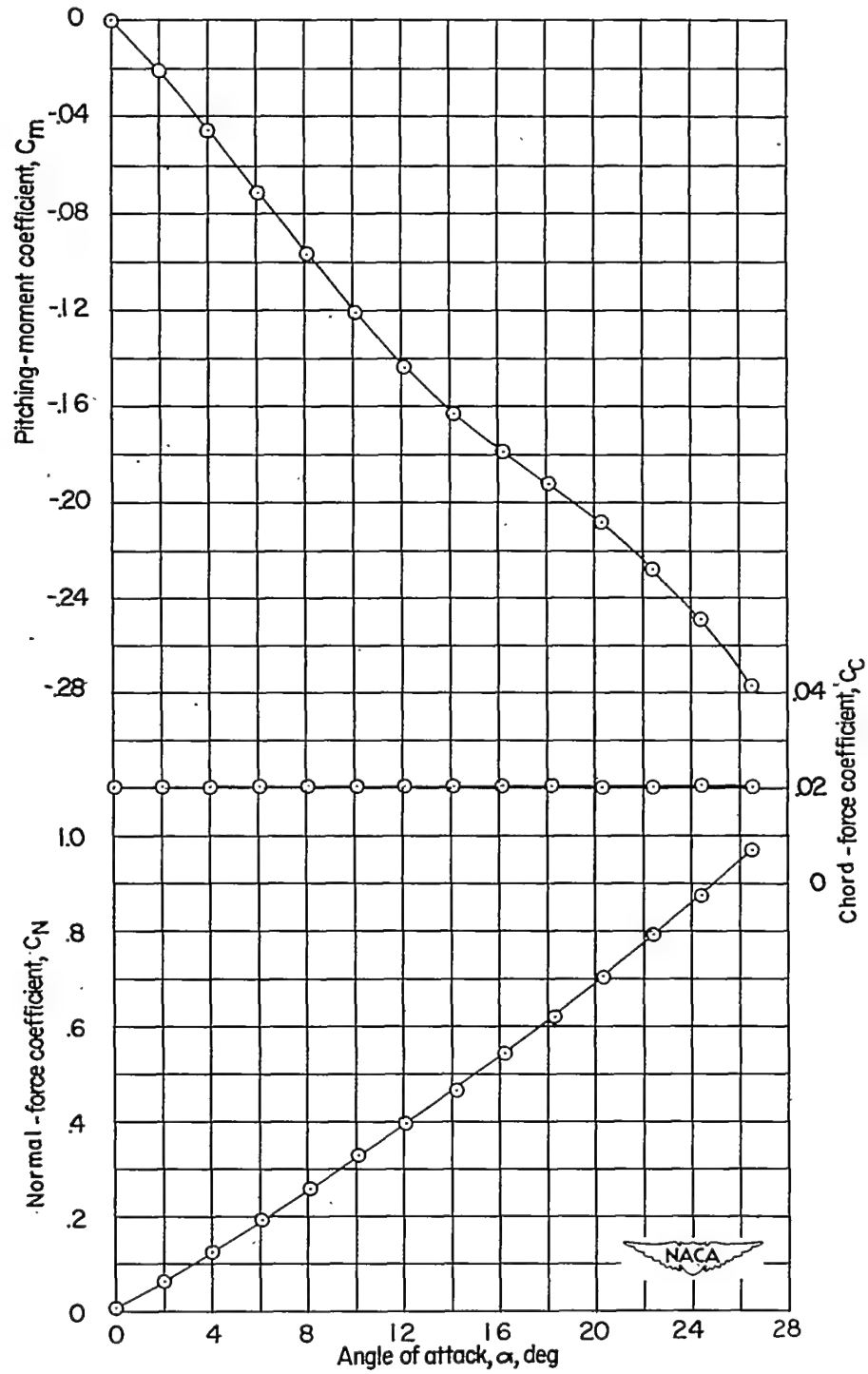

(g) Model 5; $l/d = 14.8$; $\delta_H = 0^\circ$.

Figure 3.- Concluded.

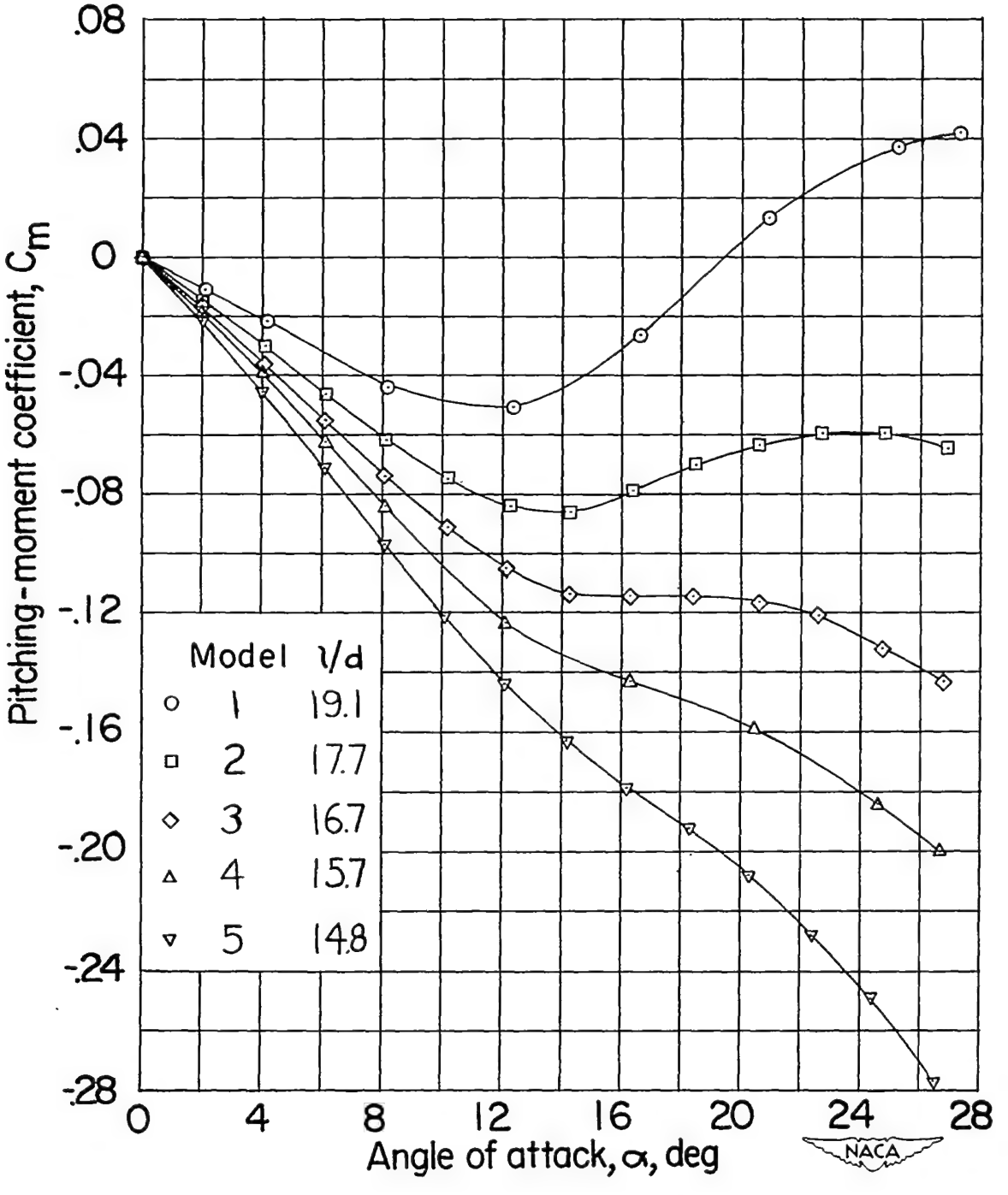

(a) Complete model; $\delta_H = 0^\circ$.

Figure 4.- Comparison of pitching-moment variation with angle of attack for various body lengths.

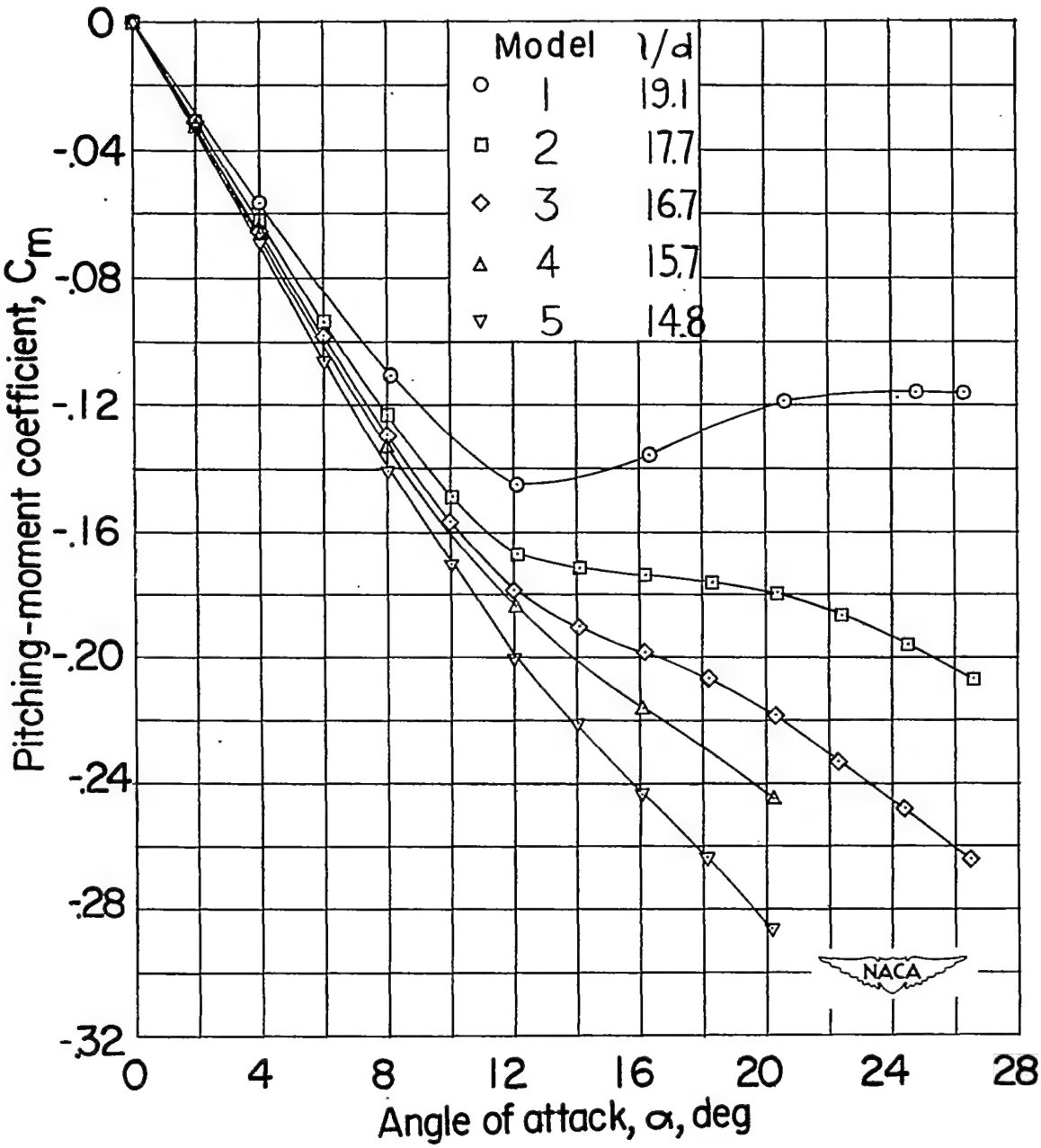

(b) Body-wing configuration.

Figure 4.- Continued.

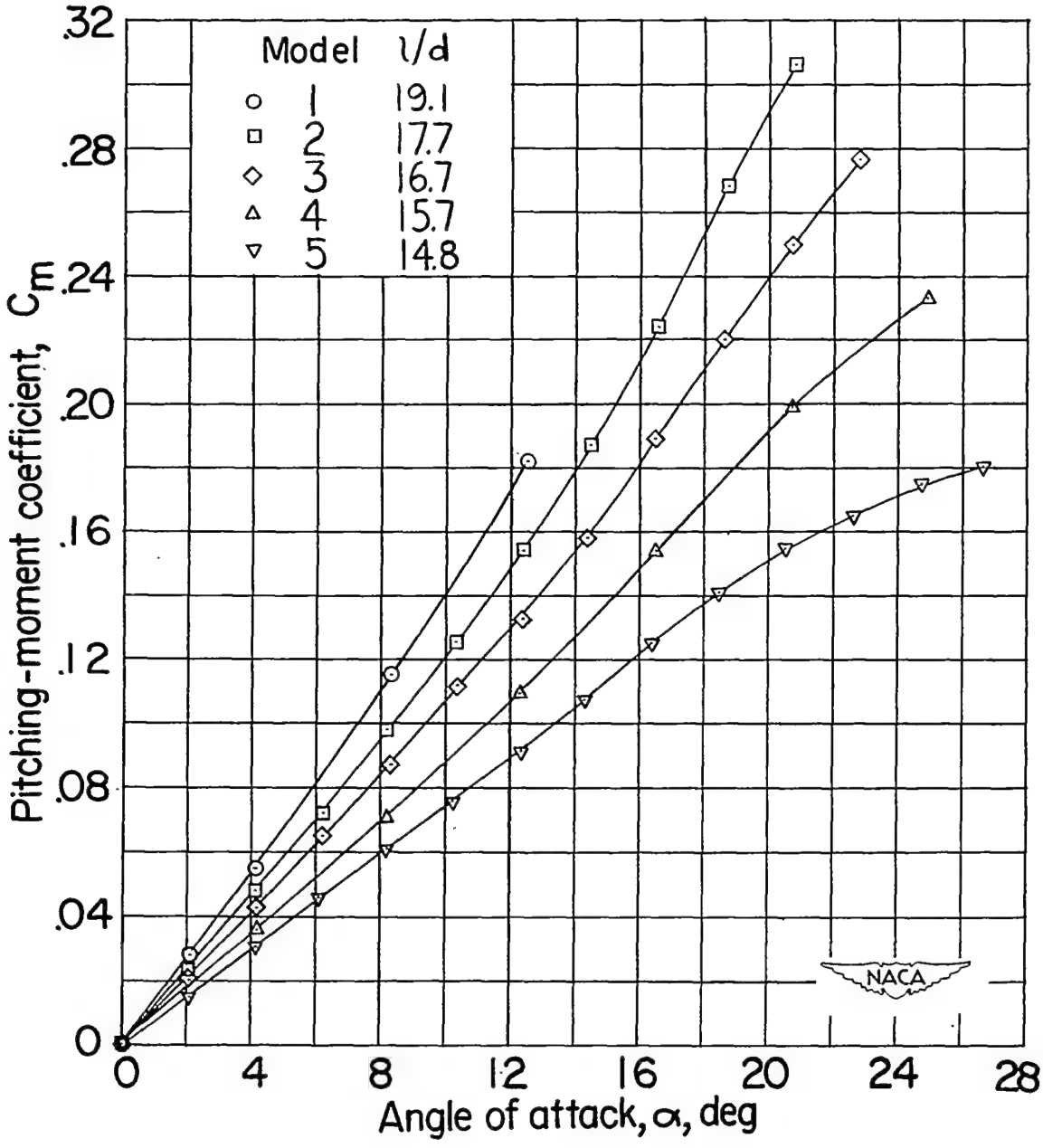

(c) Body-canard configuration; $\delta_H = 0^\circ$.

Figure 4.- Continued.

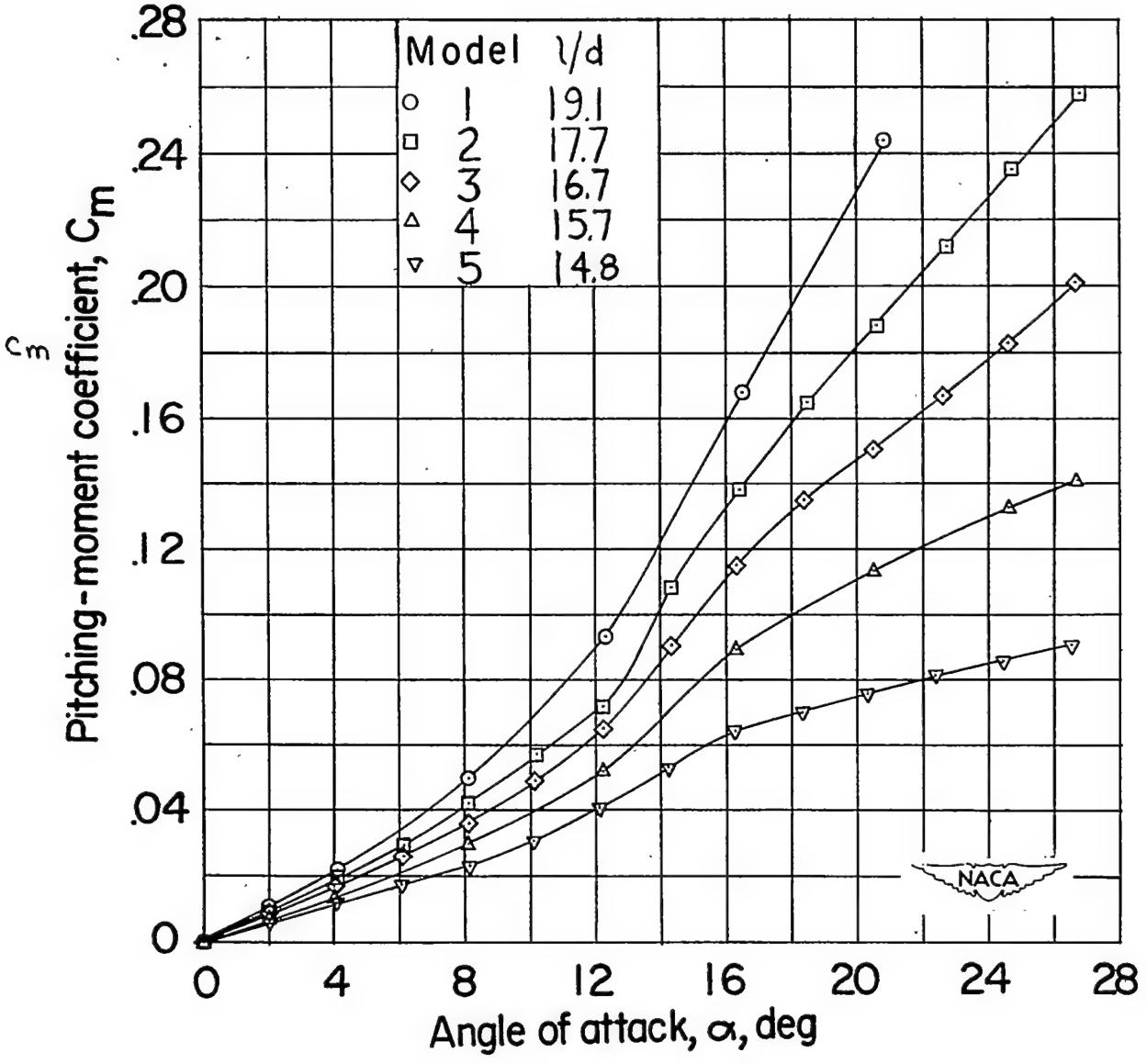

(d) Body alone.

Figure 4.- Concluded.

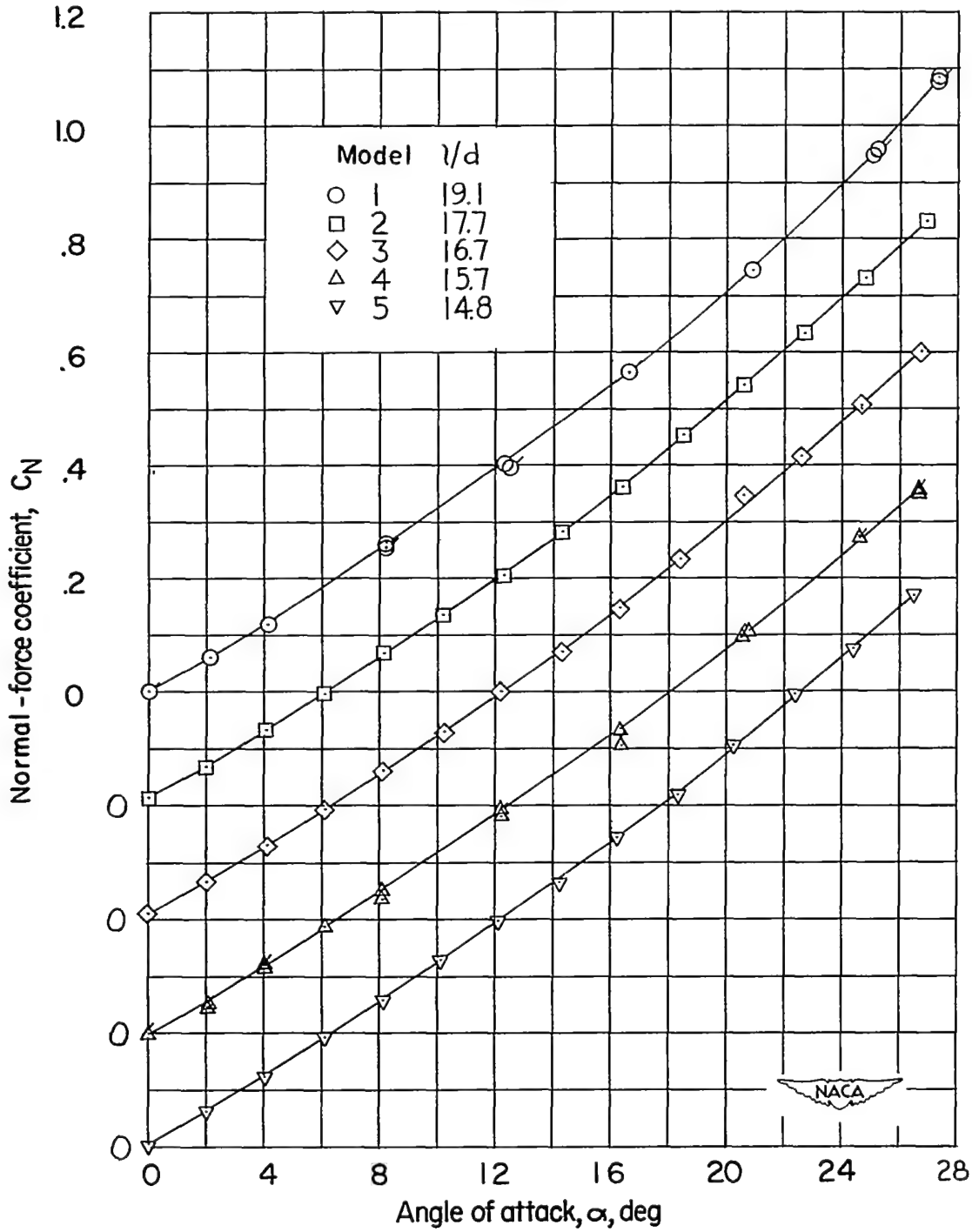

(a) Complete model; $\delta_H = 0^\circ$.

Figure 5.- Variation of normal-force coefficient with angle of attack for various models. Flagged symbols are for models with wings rotated 45°.

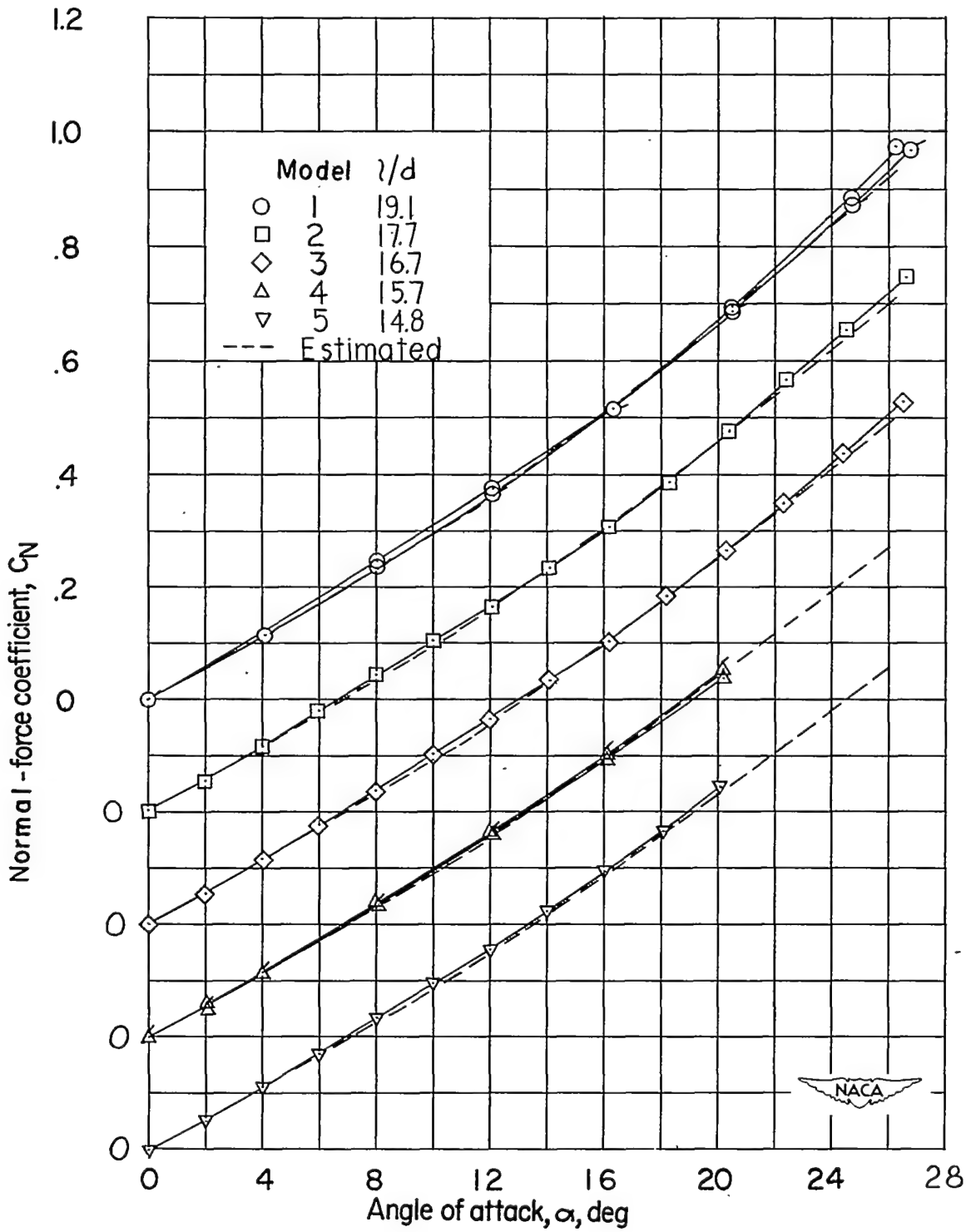

(b) Body-wing configuration.

Figure 5.- Continued.

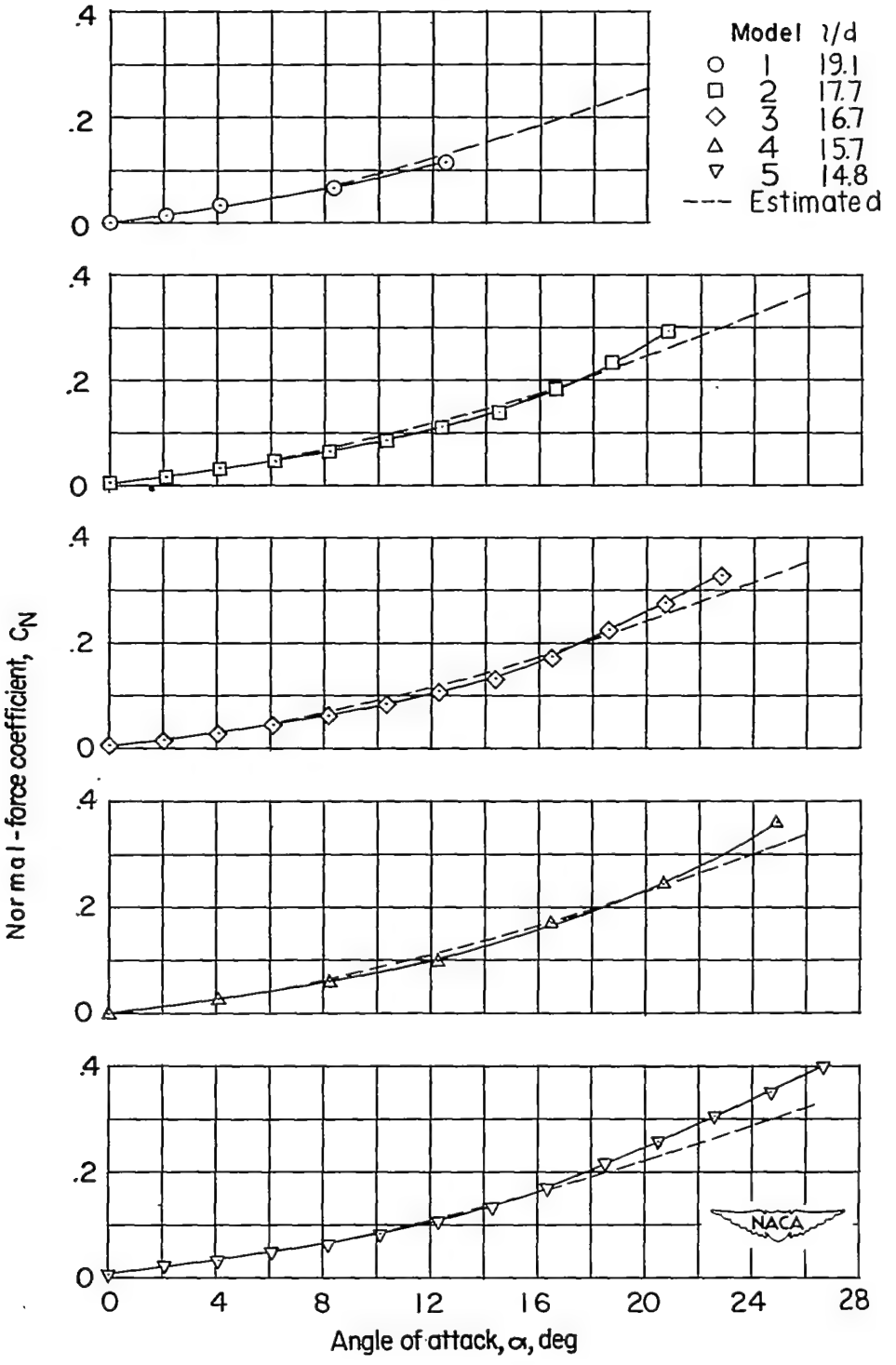

(c) Body-canard configuration, $\delta_H = 0^\circ$.

Figure 5.- Continued.

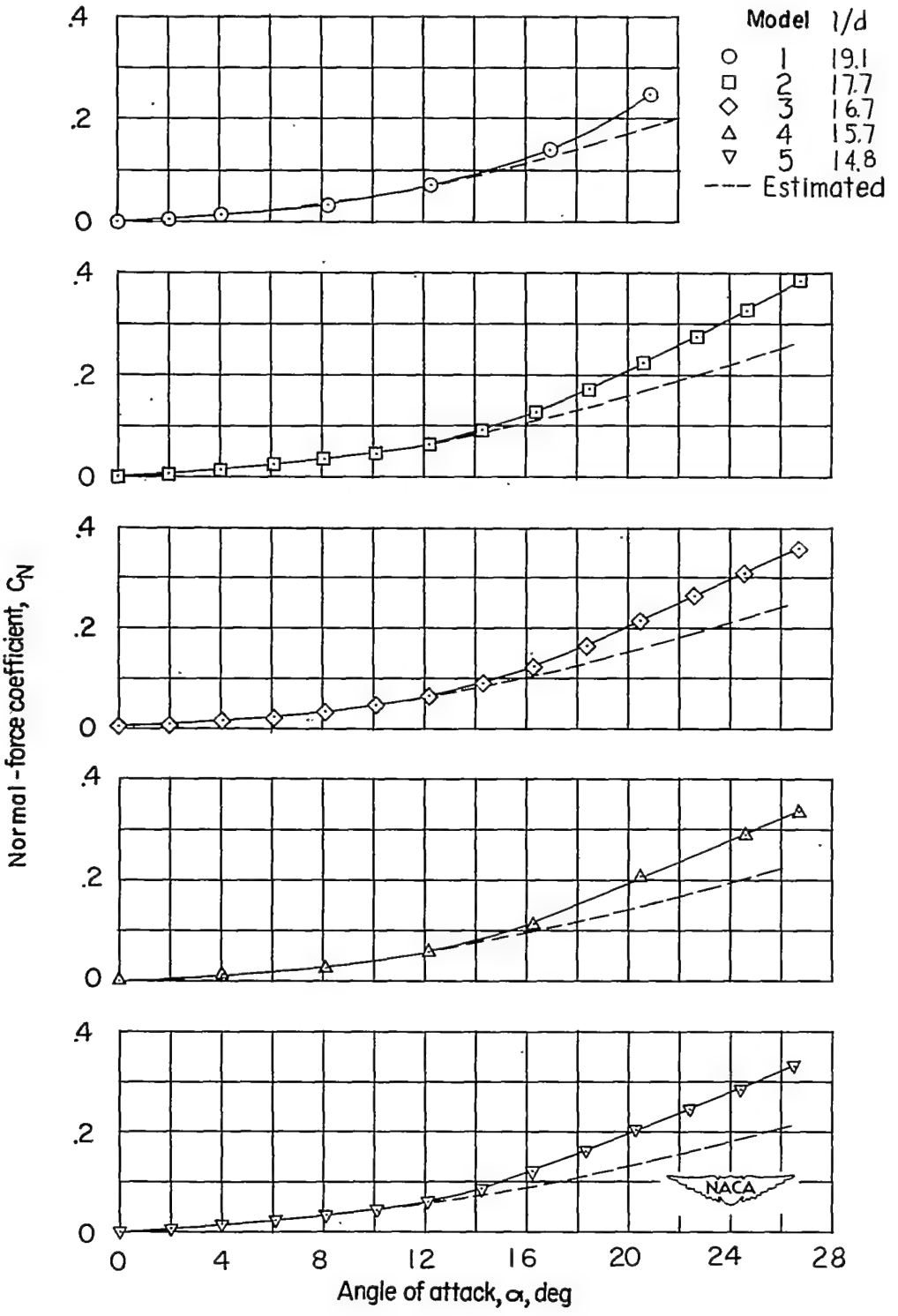

(d) Body alone.

Figure 5.- Concluded.

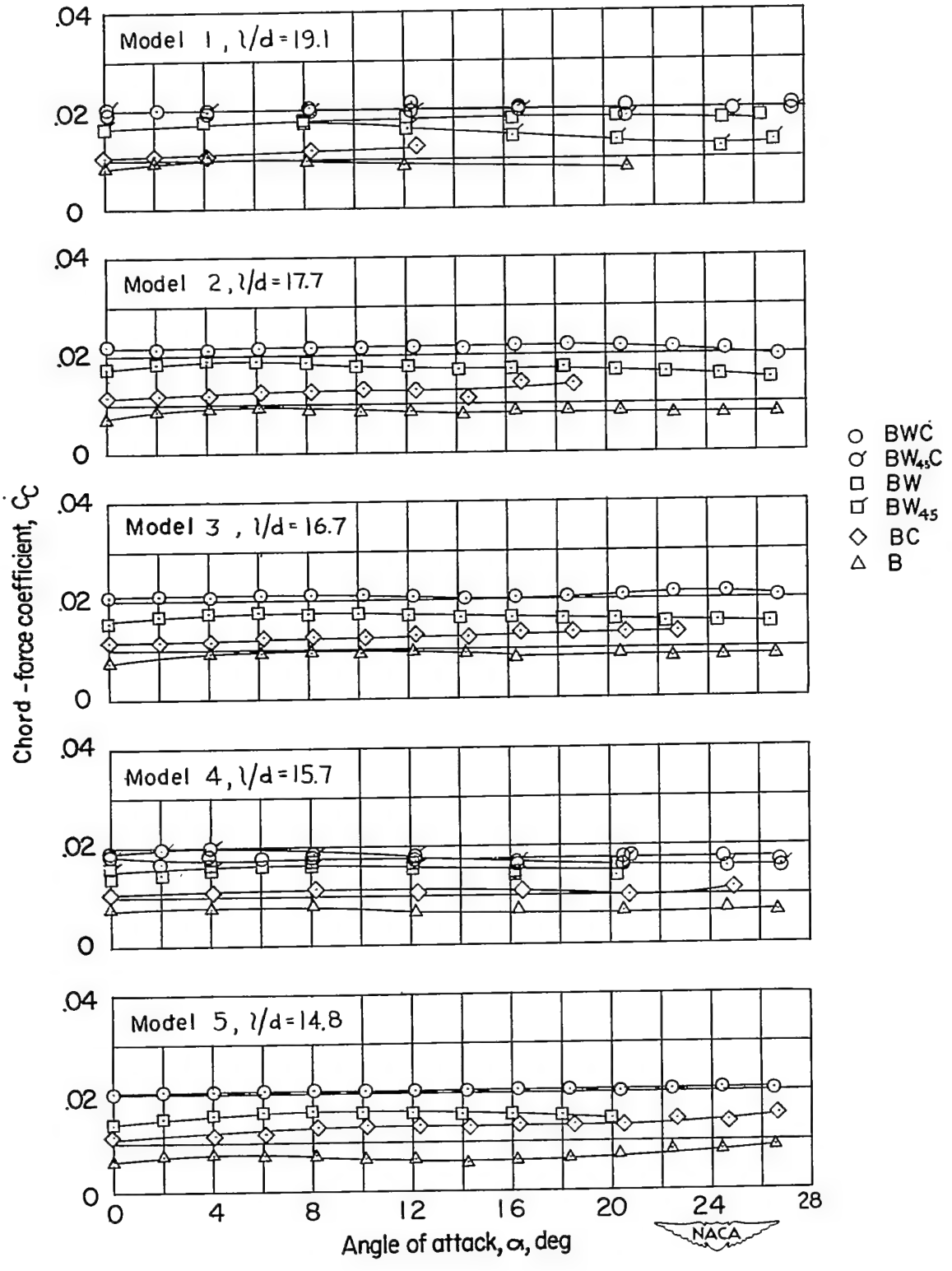

Figure 6.- Variation of chord-force coefficient with angle of attack for various configurations.

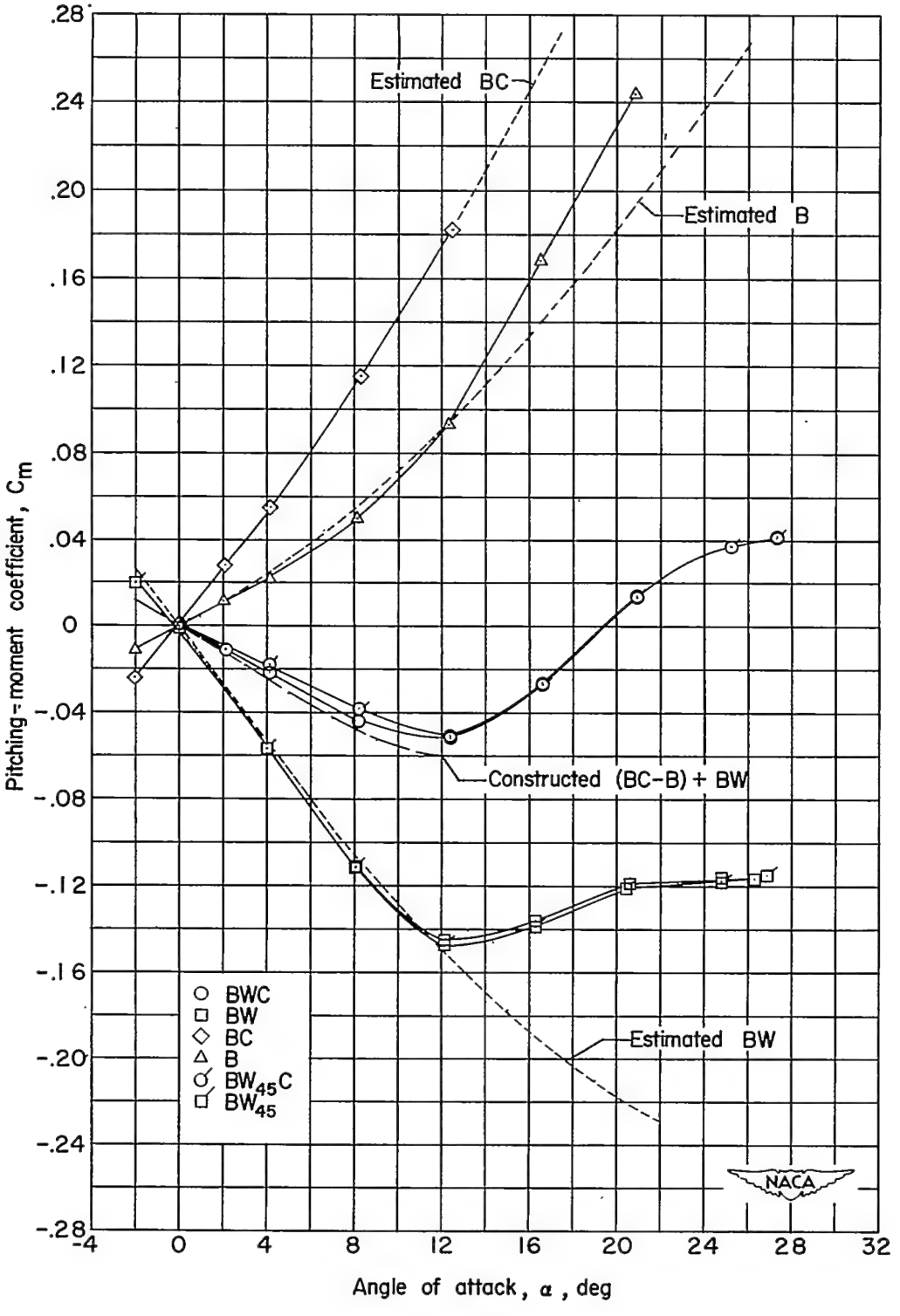

(a) Model 1; $l/d = 19.1$.

Figure 7.- Pitching-moment breakdown for various models.

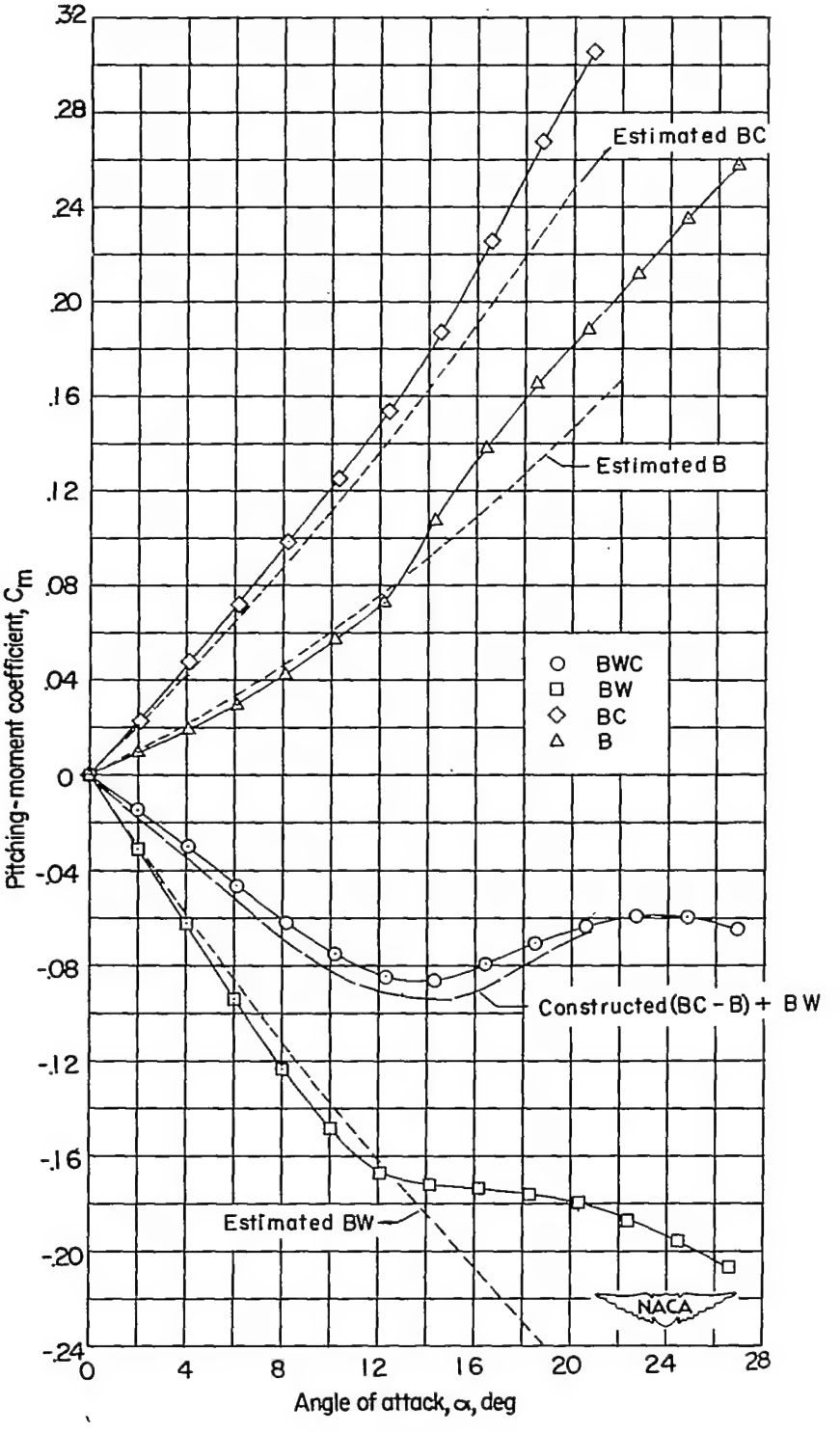

(b) Model 2; $l/d = 17.7$.

Figure 7.- Continued.

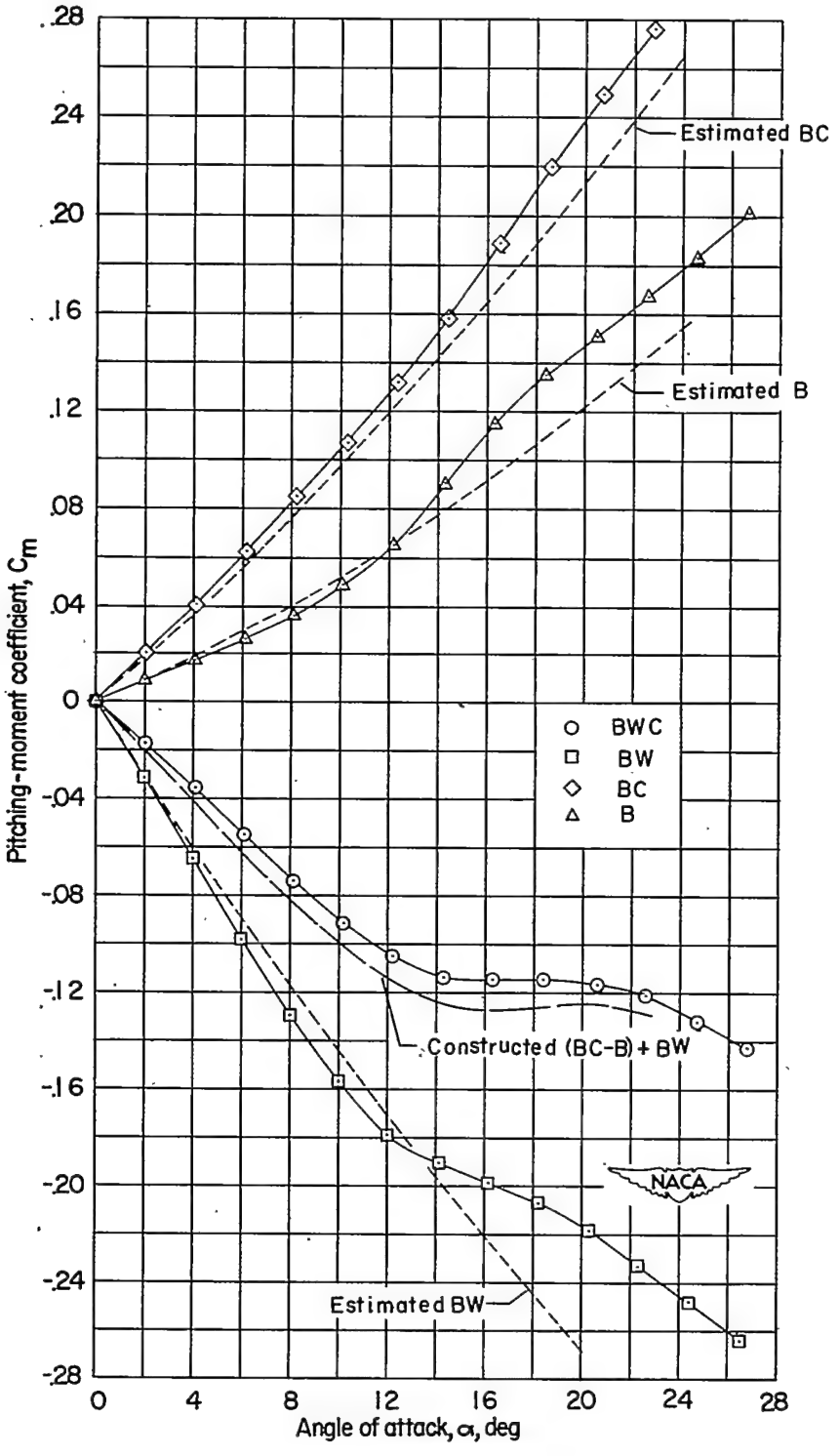

(c) Model 3; $l/d = 16.7$.

Figure 7.- Continued.

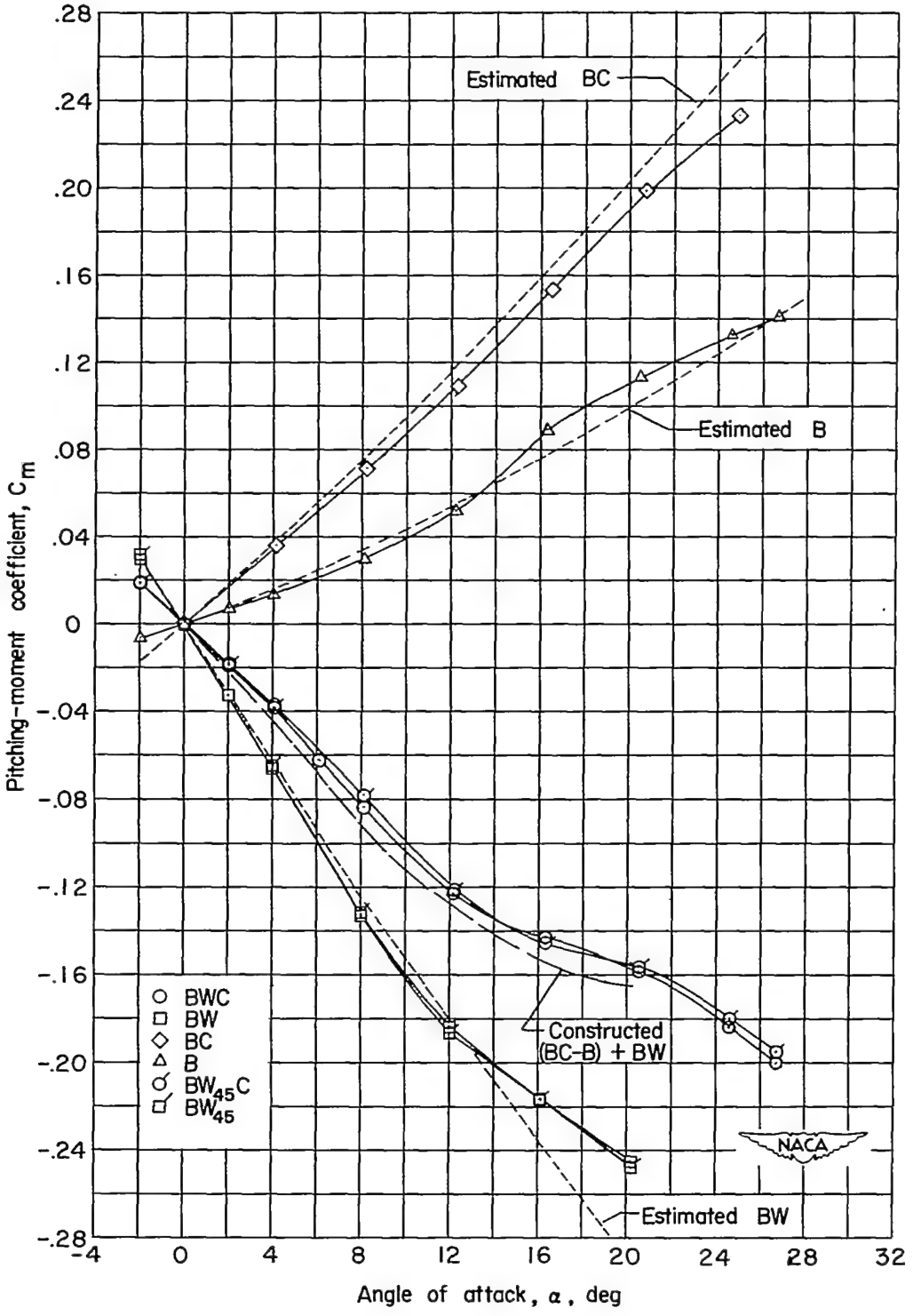

(d) Model 4; $l/d = 15.7$.

Figure 7.- Continued.

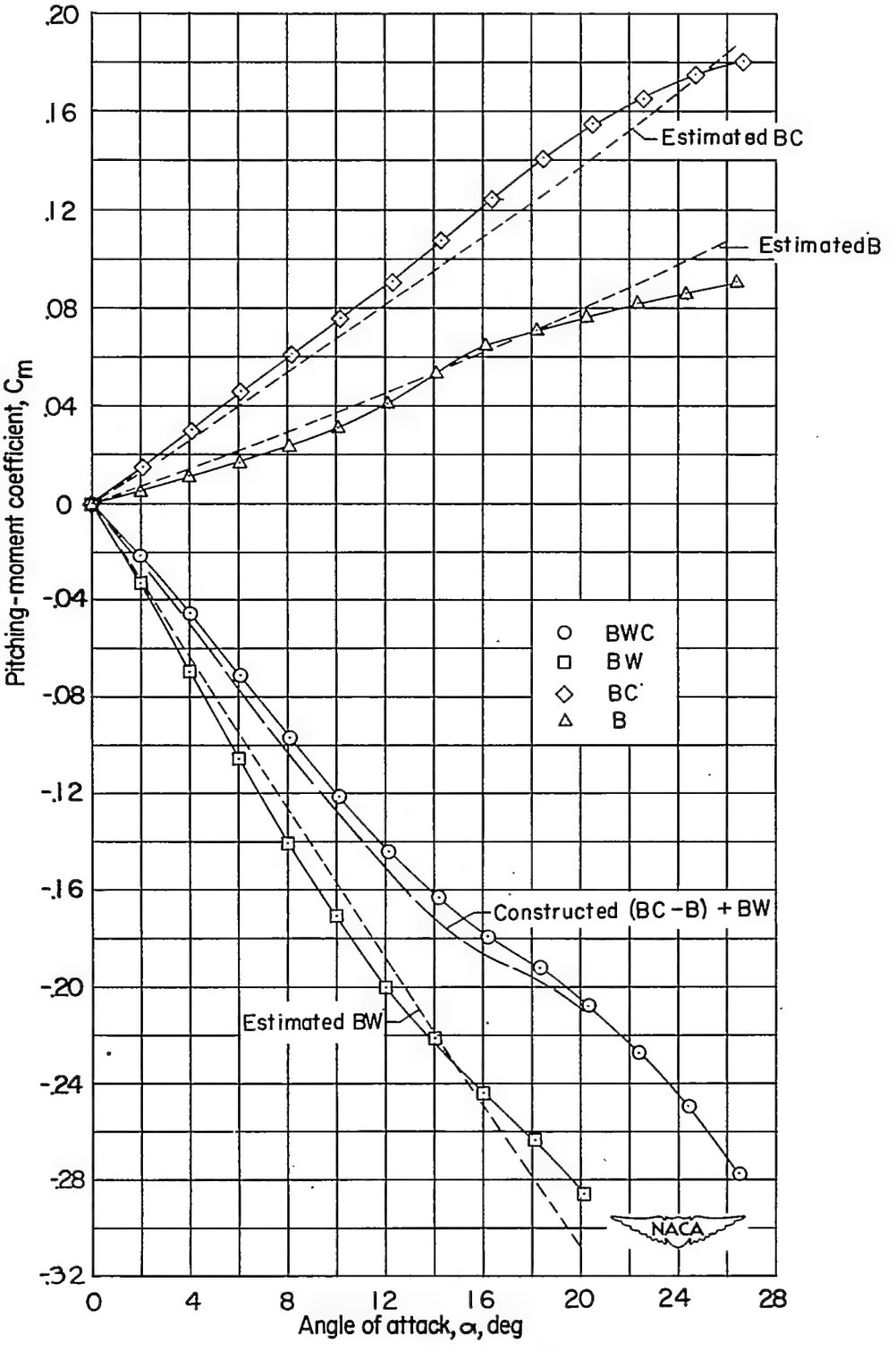

(e) Model 5; $l/d = 14.8$.

Figure 7.- Concluded.

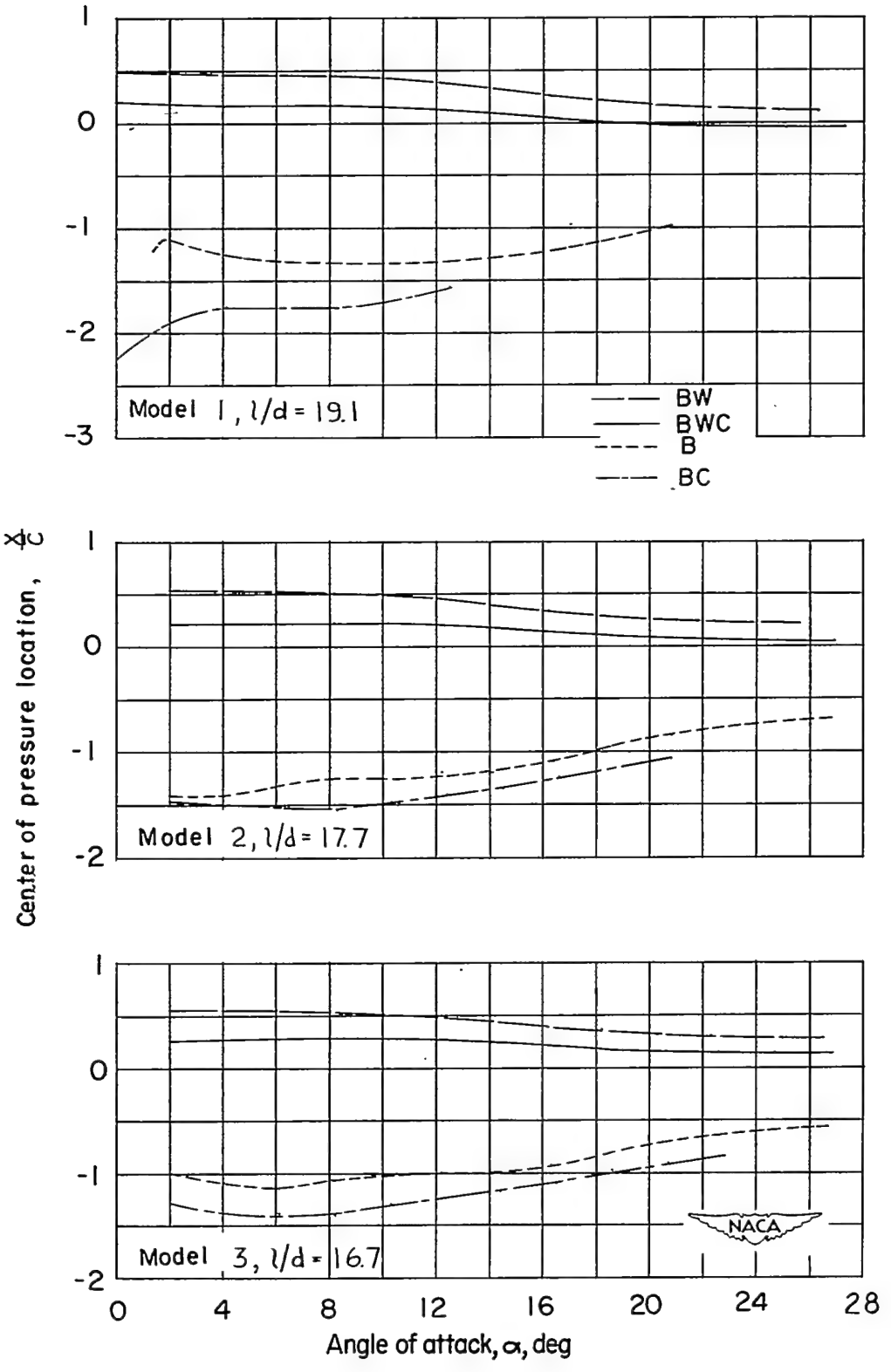

Figure 8.- Center-of-pressure locations for various configurations.

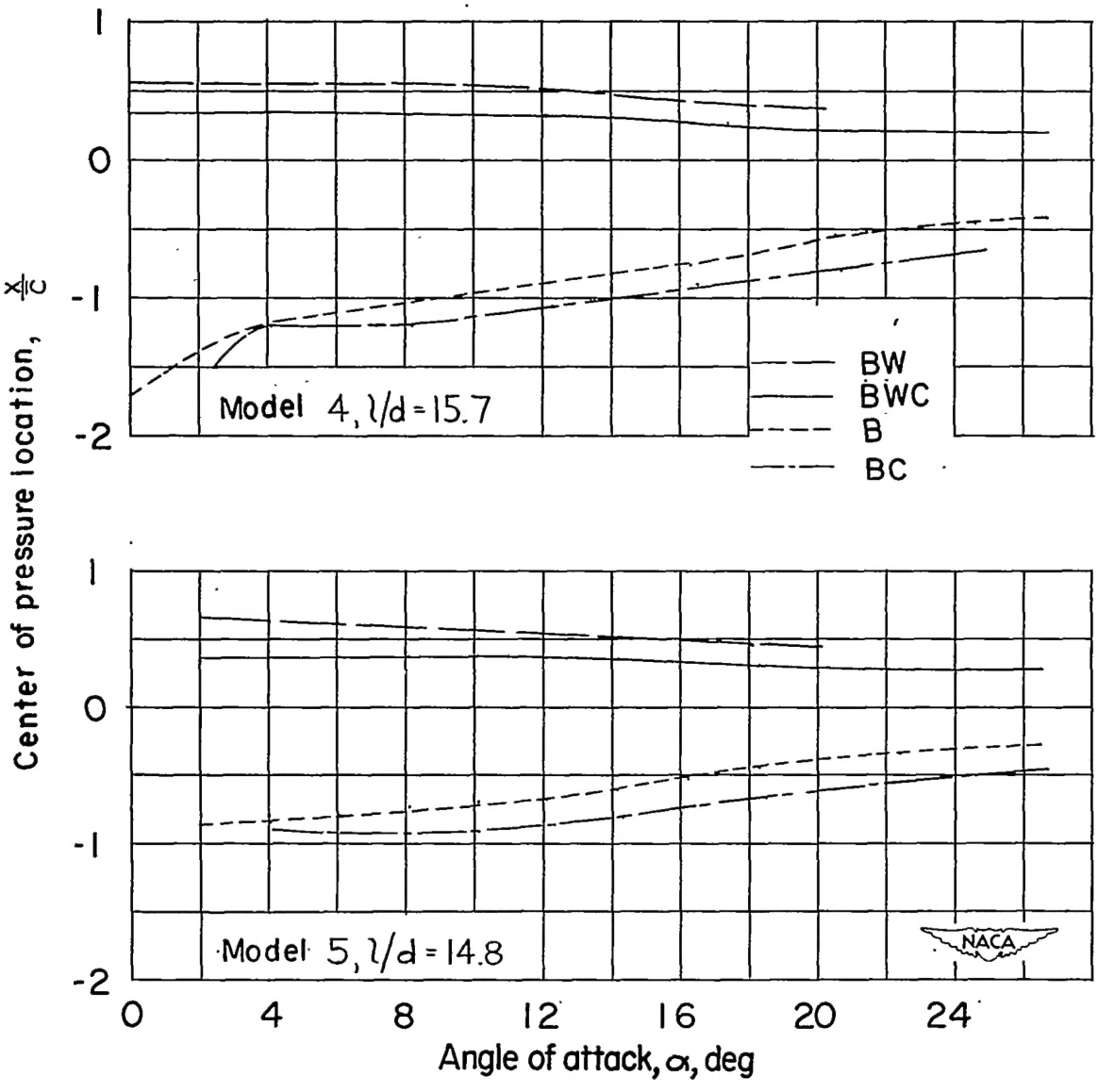

Figure 8.- Concluded.

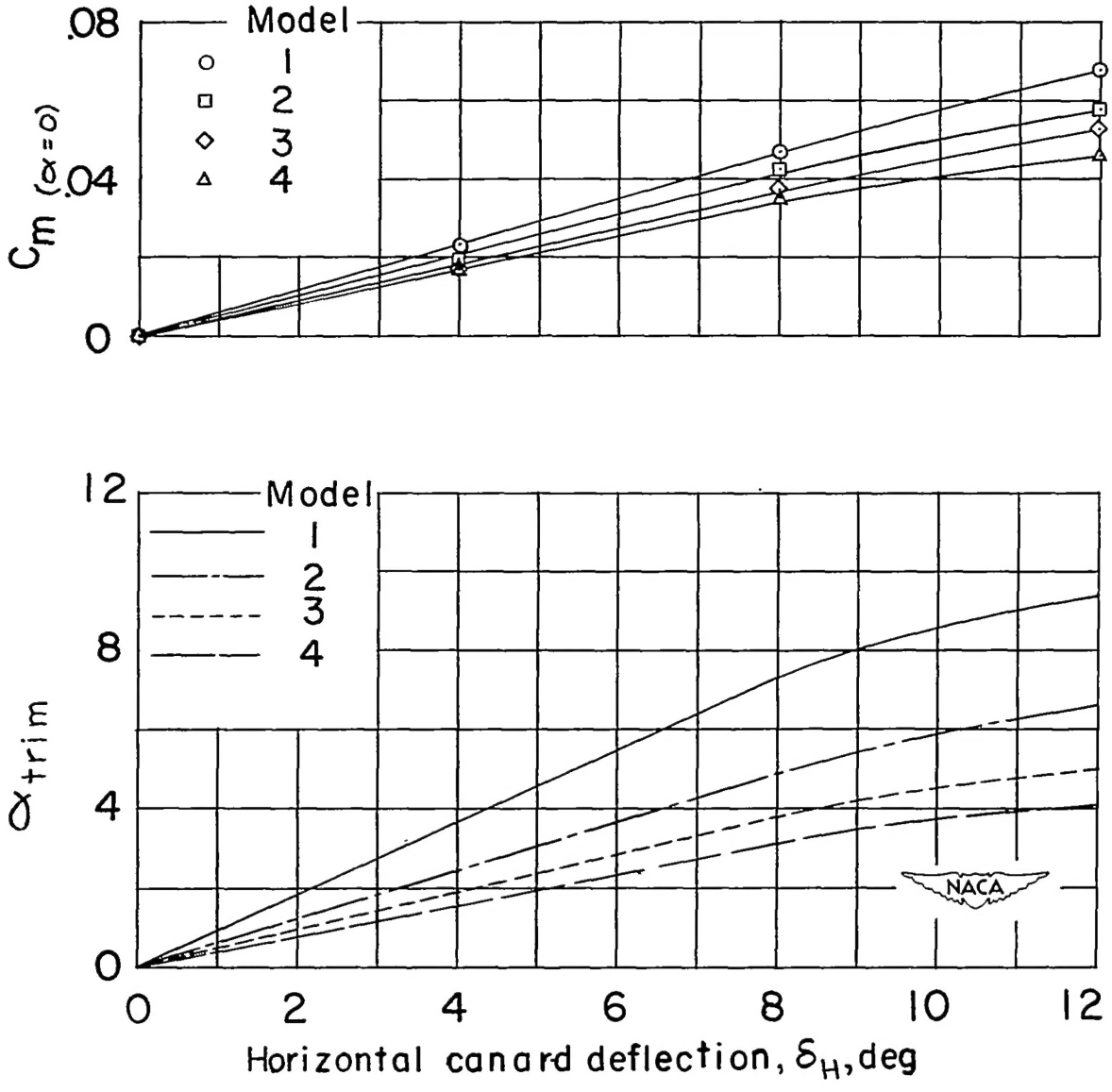

Figure 9.- Horizontal-canard-control characteristics for various models.

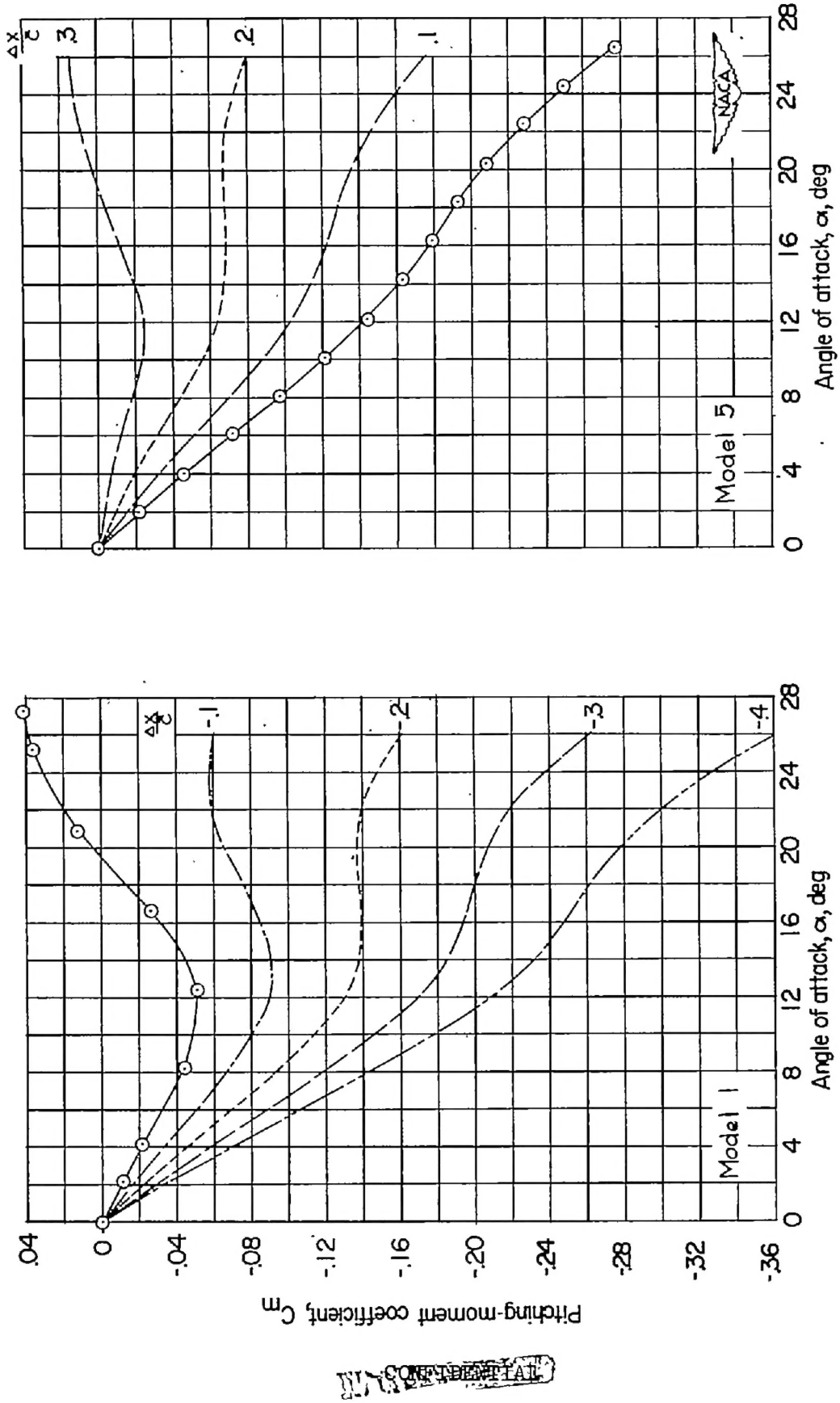

Figure 10.- Effect of center-of-gravity location on the pitching-moment characteristics of two models.

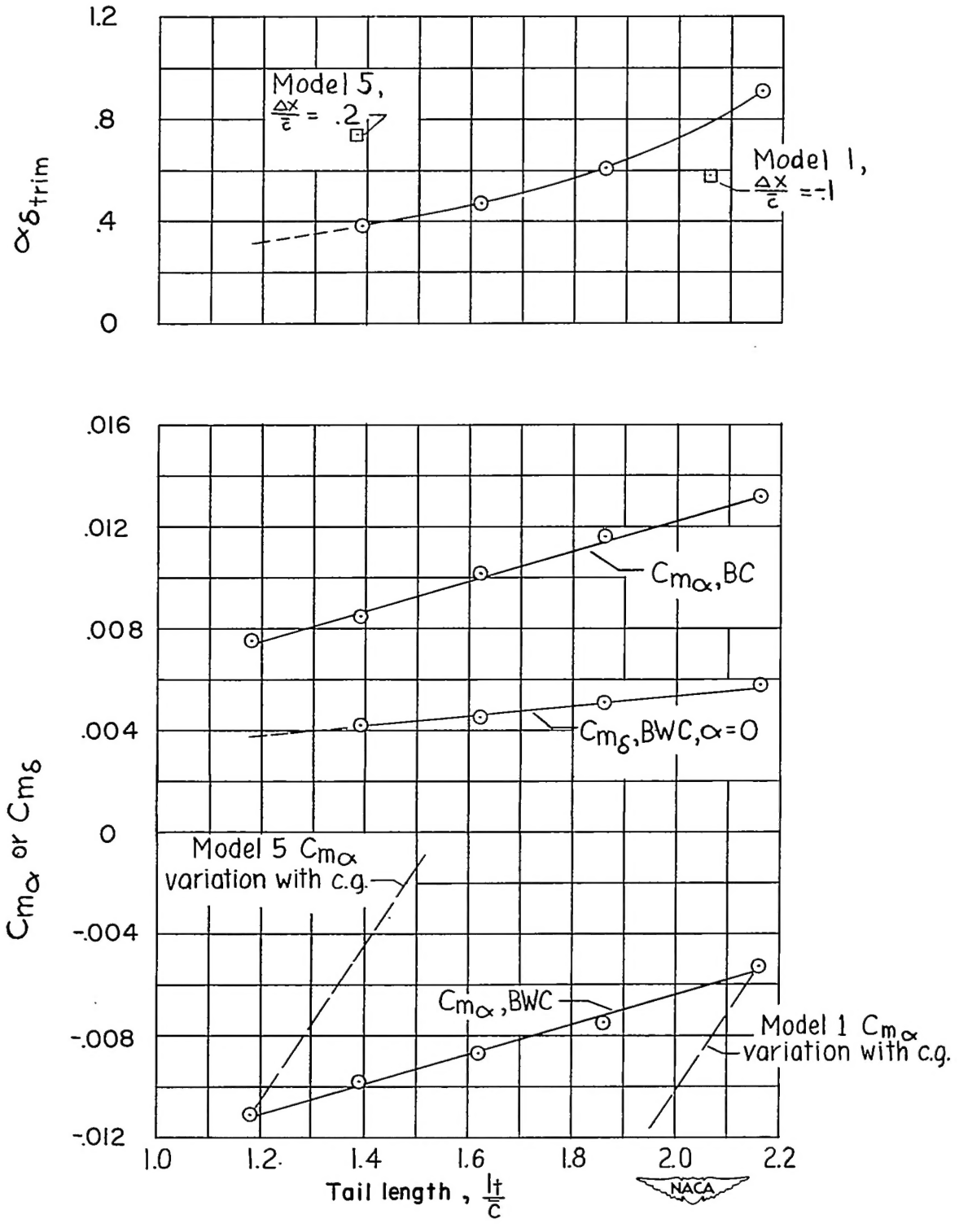

Figure 11.- Variation of C_{m_α}, C_{m_δ}, and $\alpha_{\delta_{trim}}$ with tail length.

NACA-Langley - 10-30-53 - 325